Physics-Informed Options Portfolio Construction: Arbitrage Detection, Mispricing Exploitation, and Geometric Rebalancing

Gauge-theoretic portfolio invariants, correlated Monte-Carlo optimization, Rough Heston calibration with convergence proofs, Sharpe-optimal rebalancing, and options hedging overlays.

Extended edition with full derivations, worked examples, and estimation protocols.

Melvin Alvarez-Caradu
Independent Researcher, HFThot Research Lab
https://hfthot-lab.eu

April 2026 — v3.0 (affine Volterra rewrite)

We present a unified, production-grade framework for options mispricing detection and arbitrage exploitation under affine Volterra *stochastic-volatility dynamics, spanning four algorithmic laboratories: (i) an* affine Volterra mispricing lab *that calibrates the Quintic Ornstein–Uhlenbeck model (Abi Jaber et al., 2022), the rough Hawkes Heston model (Bondi–Pulido–Scotti, 2022), and the Quadratic Rough Heston+ extension (Bourgey et al., 2026) to joint S&P 500/VIX/0DTE option surfaces, then drives Sharpe-optimal allocation through convex-duality and BSDE rebalancing rules (Alfonsi–Schied–Slynko, 2012); (ii) a* derivatives arbitrage engine *detecting vertical-spread, butterfly, and put–call parity violations across multi-asset option chains; (iii) a* cross-symbol mispricing scanner *with correlated Monte-Carlo VaR-constrained portfolio optimisation; and (iv) an* options leverage lab *constructing collars, bull/bear spreads, and iron condors whose sizing is governed by model-implied short-dated skew/curvature signatures.*
This extended edition provides complete mathematical derivations *from first principles for every closed-form result: the Black–Scholes formula via risk-neutral pricing, the Riccati–Volterra characteristic-function representation for affine Volterra models, full convergence proofs for the multi-factor Markovian approximation of rough kernels, joint SPX/VIX/0DTE calibration objectives, the Alfonsi–Schied–Slynko convex-decay characterisation of price-impact resilience, and BSDE-based optimal rebalancing under Volterra market impact. Every derivation is accompanied by a worked numerical example. All algorithms are implemented in a Streamlit-based research platform with Rust-accelerated (Rayon-parallel) pricing kernels, and a companion Jupyter notebook reproduces every numerical result, including Monte-Carlo simulation of the rough Hawkes Heston model and joint calibration of 0DTE smiles.*

Prerequisites

Required background: Stochastic calculus (Itô integral, SDE), Black–Scholes–Merton option pricing, basic portfolio theory (Markowitz), linear algebra (eigendecomposition, Cholesky factorisation). Familiarity with stochastic Volterra equations and Fourier pricing methods is helpful for Section 3 but not essential — we develop the affine Volterra theory and the Riccati–Volterra characteristic function from first principles.

Contents

1 Introduction

1.1 Motivation

The contemporary options market challenges quantitative portfolio managers on two fronts. First, combinatorial complexity: a universe of N underlyings, each with K strikes and M expiries, yields $\mathcal{O}(NKM)$ contracts whose risk/reward profiles must be evaluated jointly. Second, *model risk*: every pricing model (Black–Scholes, local volatility, Rough Heston) encodes assumptions that fail in different market regimes, creating persistent mispricings that a well-calibrated system can exploit.

This paper describes four interconnected algorithmic laboratories ("Labs") that address these challenges at production scale:

Lab 1. Affine Volterra Mispricing (§3): A jointly calibrated stochastic-volatility engine combining Markovian (Heston, Quintic Ornstein–Uhlenbeck) and non-Markovian (rough Hawkes Heston, Quadratic Rough Heston+) affine models, with Riccati–Volterra Fourier pricing and a convex-duality / BSDE Sharpe-optimal allocator targeting joint SPX/VIX/0DTE surfaces.

Lab 2. Derivatives Arbitrage (§4): A model-free arbitrage scanner detecting violations of no-arbitrage bounds (vertical spreads, butterfly convexity, put-call parity).

Lab 3. Mispricing Scanner (§5): A cross-symbol, multi-strategy optimiser combining regime-aware mispricing detection with correlated Monte-Carlo portfolio construction under VaR constraints.

Lab 4. Options Leverage (§6): A leveraged strategy builder (collars, spreads, condors) whose sizing is driven by model-implied 0DTE skew, curvature, and Zumbach-effect signatures from Lab 1.

1.2 Contributions

- A unified *affine Volterra calibration framework* (§3) combining four state-of-the-art models for joint SPX/VIX/0DTE smiles: classical Heston (baseline), the Quintic Ornstein–Uhlenbeck polynomial volatility model of Abi Jaber et al. (3), the rough Hawkes Heston model of Bondi et al. (5), and the Quadratic Rough Heston+ extension of Bourgey et al. (6), all expressed through a common Riccati–Volterra characteristic-function pipeline.
- An explicit *multi-factor Markovian approximation* of fractional kernels that converts non-Markovian rough volatility into a finite-dimensional ODE system suitable for Rust/Rayon-parallel Monte-Carlo and Fourier pricing (Theorem 3.2).
- A *convex-duality + BSDE rebalancing rule* derived from the Alfonsi–Schied–Slynko characterisation of admissible price-impact decay (7), providing Sharpe-optimal weights under a Volterra propagator market-impact constraint (Proposition 3.3).
- A *0DTE leverage decision rule* that maps the QRH+ boosting parameter b_0 and skew-stickiness ratio (SSR) into position sizes for collars, spreads, and iron condors (§6), connecting Lab 1 model diagnostics to Lab 4 execution.
- A *greedy portfolio construction* with correlated Cholesky Monte-Carlo VaR checking that provably respects budget and tail-risk constraints (Algorithm 1).

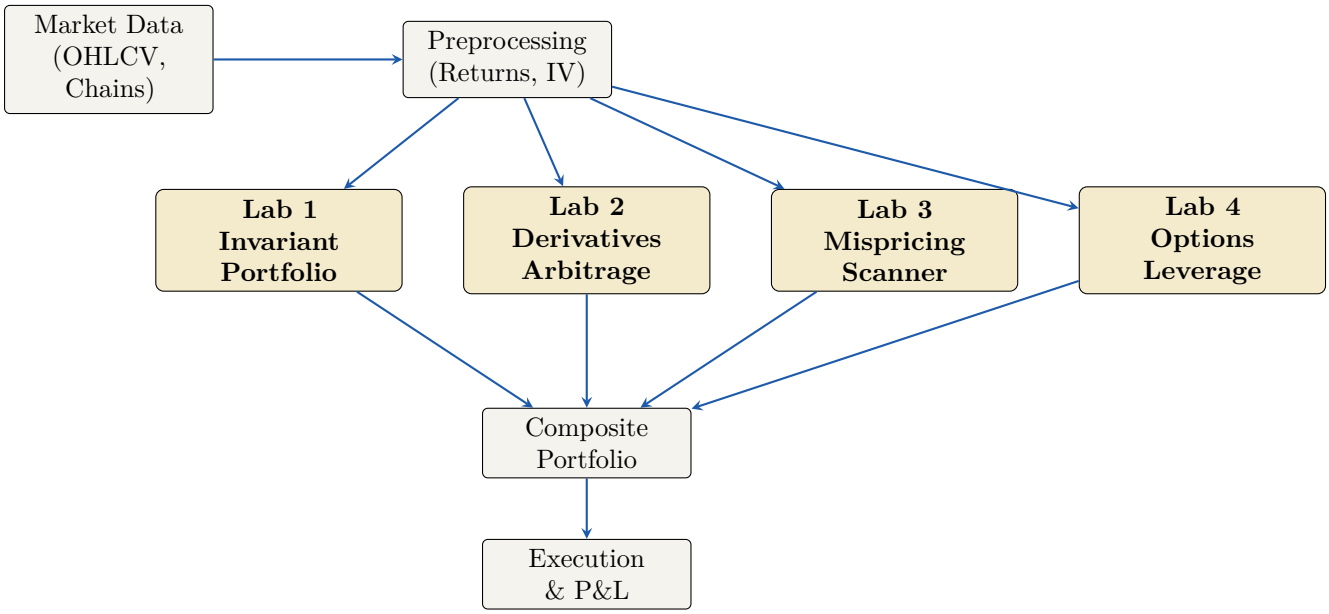

Figure 1: Architecture of the four-lab framework: market data flows through preprocessing into four specialised laboratories, whose outputs are combined into a composite portfolio for execution.

- End-to-end calibration pipelines from Yahoo Finance / CBOE data to executable orders, with explicit cost analysis and P&L range visualisations.
- Rust-accelerated (Rayon) rough-volatility pricing achieving $> 50\times$ speedup with full convergence proof (Theorem 2.6).

1.3 Paper Organisation

Section 2 develops the mathematical foundations from first principles: Black–Scholes pricing via risk-neutral valuation (with full derivation of the PDE and closed-form solution), Greek sensitivities, Rough Heston dynamics with convergence proof, and Ornstein–Uhlenbeck/Hurst estimation protocols. Sections 3–6 present the four labs, each following a uniform template: mathematical framework, calibration procedure, risk estimation, and worked examples. Section 7 details the backtesting methodology, §8 consolidates execution considerations, §9 presents the statistical inference and estimation framework, §10 provides convergence analysis for all numerical methods, and §11 concludes with future directions. Appendices provide algorithmic pseudocode, additional proofs, and a compilation of all Greek and P&L formulas.

2 Mathematical Preliminaries

2.1 Probability Foundations

Definition 2.1 (Filtered probability space)**.** A *filtered probability space* $(\Omega, \mathcal{F}, \{\mathcal{F}_t\}_{t\geq 0}, \mathbb{P})$ consists of a sample space Ω, a σ-algebra $\mathcal{F}$, an increasing filtration $\mathcal{F}_0 \subset \mathcal{F}_1 \subset \cdots \subset \mathcal{F}$ representing information flow, and a probability measure $\mathbb{P} : \mathcal{F} \to [0, 1]$.

Theorem 2.1 (First Fundamental Theorem of Asset Pricing)**.** *A frictionless market with finitely many securities is arbitrage-free if and only if there exists a probability measure* $\mathbb{Q} \sim \mathbb{P}$ *(equivalent*

martingale measure) under which all discounted asset prices $\tilde{S}_t = e^{-rt}S_t$ are $\mathbb{Q}$-martingales:

$$\tilde{S}_t = \mathbb{E}^{\mathbb{Q}}[\tilde{S}_T \mid \mathcal{F}_t], \quad 0 \le t \le T.$$

The change of measure from $\mathbb{P}$ to $\mathbb{Q}$ is governed by the Radon–Nikodym derivative (or **Girsanov kernel**):

$$\left.\frac{d\mathbb{Q}}{d\mathbb{P}}\right|_{\mathcal{F}_t} = \exp\!\Big(-\int_0^t \theta_s \,\mathrm{d}W_s - \frac{1}{2}\int_0^t \theta_s^2 \,\mathrm{d}s\Big), \quad \theta_t = \frac{\mu - r}{\sigma} \text{ (market price of risk).} \tag{1}$$

Theorem 2.2 (Girsanov's theorem)**.** *Under the measure $\mathbb{Q}$ defined by (1), the process $W_t^{\mathbb{Q}} = W_t + \int_0^t \theta_s \,\mathrm{d}s$ is a $\mathbb{Q}$-Brownian motion. In particular, $\mathrm{d}S_t = rS_t\,\mathrm{d}t + \sigma S_t\,\mathrm{d}W_t^{\mathbb{Q}}$.*

2.2 Black–Scholes Framework — Full Derivation

Under the physical measure $\mathbb{P}$, the stock follows geometric Brownian motion:

$$\mathrm{d}S_t = \mu S_t\,\mathrm{d}t + \sigma S_t\,\mathrm{d}W_t. \tag{2}$$

2.2.1 Itô's Lemma

Theorem 2.3 (Itô's lemma)**.** *Let $f \in C^{1,2}([0,T]\times\mathbb{R})$ and let X_t satisfy $\mathrm{d}X_t = a_t\,\mathrm{d}t + b_t\,\mathrm{d}W_t$. Then*

$$\mathrm{d}f(t,X_t) = \left(\frac{\partial f}{\partial t} + a_t\frac{\partial f}{\partial x} + \frac{1}{2}b_t^2\frac{\partial^2 f}{\partial x^2}\right)\mathrm{d}t + b_t\frac{\partial f}{\partial x}\,\mathrm{d}W_t. \tag{3}$$

Proof sketch. Expand $f(t+\mathrm{d}t, X_t+\mathrm{d}X_t)$ via Taylor to second order in $\mathrm{d}X_t$ and first order in $\mathrm{d}t$. Use the rules $(\mathrm{d}W_t)^2 = \mathrm{d}t$, $\mathrm{d}t\cdot\mathrm{d}W_t = 0$, $(\mathrm{d}t)^2 = 0$ (which follow from the quadratic variation of Brownian motion). □

2.2.2 Log-Normal Solution

Apply Itô to $f(t,S) = \ln S$ with $a = \mu S$, $b = \sigma S$:

$$\mathrm{d}(\ln S_t) = \frac{1}{S_t}\,\mathrm{d}S_t - \frac{1}{2}\frac{1}{S_t^2}(\sigma S_t)^2\,\mathrm{d}t = \left(\mu - \tfrac{1}{2}\sigma^2\right)\mathrm{d}t + \sigma\,\mathrm{d}W_t. \tag{4}$$

Integrating from 0 to T:

$$\ln S_T = \ln S_0 + \left(\mu - \tfrac{1}{2}\sigma^2\right)T + \sigma W_T. \tag{5}$$

Hence $\ln S_T \sim \mathcal{N}\big(\ln S_0 + (\mu - \sigma^2/2)T,\ \sigma^2 T\big)$ and

$$S_T = S_0 \exp\!\Big\{\left(\mu - \tfrac{1}{2}\sigma^2\right)T + \sigma W_T\Big\}. \tag{6}$$

2.2.3 The Black–Scholes PDE via Delta Hedging

Consider a derivative $V(t,S)$ on the stock. Construct a hedging portfolio:

$$\Pi_t = V(t,S_t) - \Delta_t\, S_t, \tag{7}$$

where Δ_t is the hedge ratio to be determined. By Itô:

$$\begin{aligned}\mathrm{d}\Pi_t &= \mathrm{d}V - \Delta\,\mathrm{d}S \\ &= \left(\frac{\partial V}{\partial t} + \mu S\frac{\partial V}{\partial S} + \frac{1}{2}\sigma^2 S^2\frac{\partial^2 V}{\partial S^2}\right)\mathrm{d}t + \sigma S\frac{\partial V}{\partial S}\,\mathrm{d}W_t - \Delta(\mu S\,\mathrm{d}t + \sigma S\,\mathrm{d}W_t).\end{aligned} \tag{8}$$

Choose $\Delta = \partial V/\partial S$ to eliminate the stochastic term:

$$\mathrm{d}\Pi_t = \left(\frac{\partial V}{\partial t} + \frac{1}{2}\sigma^2 S^2 \frac{\partial^2 V}{\partial S^2}\right) \mathrm{d}t. \tag{9}$$

This portfolio is instantaneously riskless. By no-arbitrage, $\mathrm{d}\Pi_t = r\Pi_t\,\mathrm{d}t$, so

$$\frac{\partial V}{\partial t} + \frac{1}{2}\sigma^2 S^2 \frac{\partial^2 V}{\partial S^2} = r\left(V - S\frac{\partial V}{\partial S}\right). \tag{10}$$

Rearranging gives the **Black–Scholes PDE**:

$$\boxed{\frac{\partial V}{\partial t} + \frac{1}{2}\sigma^2 S^2 \frac{\partial^2 V}{\partial S^2} + rS\frac{\partial V}{\partial S} - rV = 0.} \tag{11}$$

Key Insight

The drift μ does *not* appear in the PDE. The derivative price is independent of the investor's risk preferences — this is the essence of risk-neutral pricing.

2.2.4 Solution via Feynman–Kac

Theorem 2.4 (Feynman–Kac representation)**.** *The solution to the BS PDE* (11) *with terminal condition* $V(T,S) = h(S)$ *is*

$$V(t,S) = e^{-r(T-t)}\mathbb{E}^{\mathbb{Q}}[h(S_T) \mid S_t = S], \tag{12}$$

where under $\mathbb{Q}$, $\mathrm{d}S_t = rS_t\,\mathrm{d}t + \sigma S_t\,\mathrm{d}W_t^{\mathbb{Q}}$.

For a European call, $h(S) = \max(S-K,0) = (S-K)^+$:

$$C = e^{-rT}\mathbb{E}^{\mathbb{Q}}[(S_T - K)^+]. \tag{13}$$

Under $\mathbb{Q}$: $\ln S_T \sim \mathcal{N}(\ln S_0 + (r - \sigma^2/2)T,\ \sigma^2 T)$. Let $Z = \frac{\ln S_T - \ln S_0 - (r-\sigma^2/2)T}{\sigma\sqrt{T}} \sim \mathcal{N}(0,1)$. Then $S_T > K$ iff $Z > -d_2$ where $d_2 = \frac{\ln(S_0/K) + (r-\sigma^2/2)T}{\sigma\sqrt{T}}$.

Evaluating the expectation:

$$\begin{aligned}\mathbb{E}^{\mathbb{Q}}[(S_T-K)^+] &= \int_{-d_2}^{\infty} (S_0 e^{(r-\sigma^2/2)T + \sigma\sqrt{T}z} - K)\phi(z)\,\mathrm{d}z \\ &= S_0 e^{rT}\int_{-d_2}^{\infty} e^{-\sigma^2 T/2 + \sigma\sqrt{T}z}\phi(z)\,\mathrm{d}z - K\,\Phi(d_2).\end{aligned} \tag{14}$$

For the first integral, complete the square in the exponent:

$$-\frac{\sigma^2 T}{2} + \sigma\sqrt{T}z - \frac{z^2}{2} = -\frac{1}{2}(z - \sigma\sqrt{T})^2 + 0. \tag{15}$$

Hence:

$$\int_{-d_2}^{\infty} e^{-\sigma^2 T/2 + \sigma\sqrt{T}z}\phi(z)\,\mathrm{d}z = \int_{-d_2}^{\infty} \frac{1}{\sqrt{2\pi}} e^{-(z-\sigma\sqrt{T})^2/2}\,\mathrm{d}z = \Phi(d_2 + \sigma\sqrt{T}) = \Phi(d_1), \tag{16}$$

where $d_1 = d_2 + \sigma\sqrt{T} = \frac{\ln(S_0/K) + (r+\sigma^2/2)T}{\sigma\sqrt{T}}$.

Substituting back into (14):

$$\boxed{C_{\mathrm{BS}}(S_0, K, T, r, \sigma) = S_0\,\Phi(d_1) - Ke^{-rT}\Phi(d_2).} \tag{17}$$

2.2.5 Put-Call Parity from First Principles

Consider two portfolios at time 0:

- **Portfolio A**: long call C + bond worth Ke^{-rT}.
- **Portfolio B**: long put P + stock S_0.

At time T: $A_T = \max(S_T - K, 0) + K = \max(S_T, K)$ and $B_T = \max(K - S_T, 0) + S_T = \max(S_T, K)$. By the law of one price, $C + Ke^{-rT} = P + S_0$, whence:

$$C - P = S_0 - Ke^{-rT}. \tag{18}$$

Example 2.1 (Black–Scholes computation)**.** Let $S_0 = 100$, $K = 105$, $T = 0.25$, $r = 0.05$, $\sigma = 0.20$.

$$\begin{aligned} d_1 &= \frac{\ln(100/105) + (0.05 + 0.02) \times 0.25}{0.20\sqrt{0.25}} = \frac{-0.04879 + 0.0175}{0.10} = -0.3129, \\ d_2 &= -0.3129 - 0.10 = -0.4129, \\ \Phi(d_1) &= \Phi(-0.3129) \approx 0.3772, \quad \Phi(d_2) = \Phi(-0.4129) \approx 0.3398, \\ C &= 100 \times 0.3772 - 105\, e^{-0.0125} \times 0.3398 = 37.72 - 105 \times 0.9876 \times 0.3398 \\ &= 37.72 - 35.24 = 2.48. \end{aligned}$$

By put-call parity: $P = C - S_0 + Ke^{-rT} = 2.48 - 100 + 103.69 = 6.17$.

2.3 Greeks — Complete Derivations

2.3.1 Delta

Theorem 2.5. *The delta of a European call is* $\Delta = \Phi(d_1)$.

Proof. Differentiate $C = S\Phi(d_1) - Ke^{-rT}\Phi(d_2)$ with respect to S:

$$\frac{\partial C}{\partial S} = \Phi(d_1) + S\phi(d_1)\frac{\partial d_1}{\partial S} - Ke^{-rT}\phi(d_2)\frac{\partial d_2}{\partial S}.$$

Since d_1 and d_2 differ by a constant ($\sigma\sqrt{T}$), $\frac{\partial d_1}{\partial S} = \frac{\partial d_2}{\partial S} = \frac{1}{S\sigma\sqrt{T}}$. The key identity is $S\phi(d_1) = Ke^{-rT}\phi(d_2)$, which follows from:

$$\begin{aligned} \frac{\phi(d_1)}{\phi(d_2)} &= \exp\left(\frac{d_2^2 - d_1^2}{2}\right) = \exp\left(-\frac{(d_1 + d_2)(d_1 - d_2)}{2}\right) \\ &= \exp\left(-\frac{(d_1 + d_2)\sigma\sqrt{T}}{2}\right). \end{aligned}$$

Using $d_1 + d_2 = \frac{2\ln(S/K) + 2rT}{\sigma\sqrt{T}} - \sigma\sqrt{T}$, one verifies $\frac{S\phi(d_1)}{Ke^{-rT}\phi(d_2)} = 1$. Therefore the two chain-rule terms cancel, leaving $\Delta = \Phi(d_1)$. □

2.3.2 Gamma

$$\Gamma = \frac{\partial^2 C}{\partial S^2} = \frac{\partial \Delta}{\partial S} = \phi(d_1)\frac{\partial d_1}{\partial S} = \frac{\phi(d_1)}{S\sigma\sqrt{T}}. \tag{19}$$

Proof. Differentiate $\Delta = \Phi(d_1)$ with respect to S: $\Gamma = \phi(d_1) \cdot \frac{1}{S\sigma\sqrt{T}}$. □

2.3.3 Vega

$$\mathcal{V} = \frac{\partial C}{\partial \sigma} = S\phi(d_1)\sqrt{T}. \tag{20}$$

Proof. $\frac{\partial C}{\partial \sigma} = S\phi(d_1)\frac{\partial d_1}{\partial \sigma} - Ke^{-rT}\phi(d_2)\frac{\partial d_2}{\partial \sigma}$. With $\frac{\partial d_1}{\partial \sigma} = \frac{-d_2}{\sigma}$ and $\frac{\partial d_2}{\partial \sigma} = \frac{-d_1}{\sigma}$ (verify by direct computation), plus the identity $S\phi(d_1) = Ke^{-rT}\phi(d_2)$, we get $\mathcal{V} = S\phi(d_1)\left(\frac{-d_2+d_1}{\sigma}\right) = S\phi(d_1)\sqrt{T}$. □

2.3.4 Theta

$$\Theta = \frac{\partial C}{\partial t} = -\frac{S\phi(d_1)\sigma}{2\sqrt{T}} - rKe^{-rT}\Phi(d_2). \tag{21}$$

This follows from differentiating C with respect to t (equivalently $-T$) and using the BS PDE (11) rewritten as $\Theta + \frac{1}{2}\sigma^2 S^2\Gamma + rS\Delta - rC = 0$.

2.3.5 Rho

$$\rho = \frac{\partial C}{\partial r} = KTe^{-rT}\Phi(d_2). \tag{22}$$

Proposition 2.1 (BS PDE in terms of Greeks)**.** *The Greeks satisfy the identity:*

$$\Theta + \frac{1}{2}\sigma^2 S^2\Gamma + rS\Delta - rC = 0. \tag{23}$$

Proof. Direct substitution of $V = C$, $\partial V/\partial t = \Theta$, $\partial V/\partial S = \Delta$, $\partial^2 V/\partial S^2 = \Gamma$ into the BS PDE (11). □

For a portfolio with positions $q_\ell \in \{-1, +1\}$ and n_ℓ contracts:

$$\Delta_{\text{port}} = \sum_{\ell=1}^{L} q_\ell n_\ell \Delta_\ell, \quad \Gamma_{\text{port}} = \sum_{\ell=1}^{L} q_\ell n_\ell \Gamma_\ell, \quad \text{etc.} \tag{24}$$

Example 2.2 (Greek computation)**.** Using the parameters from Example 2.1 ($S = 100$, $K = 105$, $T = 0.25$, $r = 0.05$, $\sigma = 0.20$, $d_1 = -0.3129$, $d_2 = -0.4129$):

$$\begin{aligned}
\phi(d_1) &= \frac{1}{\sqrt{2\pi}}e^{-0.3129^2/2} \approx 0.3797,\\
\Delta &= \Phi(-0.3129) \approx 0.3772,\\
\Gamma &= \frac{0.3797}{100 \times 0.20 \times 0.50} = \frac{0.3797}{10.0} = 0.0380,\\
\mathcal{V} &= 100 \times 0.3797 \times 0.50 = 18.99,\\
\Theta &= -\frac{100 \times 0.3797 \times 0.20}{2 \times 0.50} - 0.05 \times 105 \times 0.9876 \times 0.3398 = -7.59 - 1.76 = -9.35,\\
\rho &= 105 \times 0.25 \times 0.9876 \times 0.3398 = 8.82.
\end{aligned}$$

Interpretation: A \$1 increase in S raises the call by \$0.38; a 1% increase in σ raises it by \$0.19; one day of time decay costs approximately $\Theta/365 = -0.026$.

2.4 Rough Heston Model — Full Treatment

2.4.1 Motivation

Classical Heston ($H = 0.5$) produces an ATM skew that decays as $T^{-1/2}$, while empirical data exhibit much steeper short-dated skews ($\sim T^{H-1/2}$ with $H \approx 0.1$). The Rough Heston model (17) resolves this.

2.4.2 Model Definition

Definition 2.2 (Rough Heston dynamics)**.** The stock price S_t and variance V_t evolve as:

$$\mathrm{d}S_t = S_t\sqrt{V_t}\,\mathrm{d}W_t^S, \tag{25}$$

$$V_t = V_0 + \frac{1}{\Gamma(H+\frac{1}{2})}\int_0^t (t-s)^{H-1/2}\kappa(\theta - V_s)\,\mathrm{d}s + \frac{\nu}{\Gamma(H+\frac{1}{2})}\int_0^t (t-s)^{H-1/2}\sqrt{V_s}\,\mathrm{d}W_s^V, \tag{26}$$

where $H \in (0, \frac{1}{2})$ is the Hurst index, $\kappa > 0$ the mean-reversion speed, $\theta > 0$ the long-run variance, $\nu > 0$ the vol-of-vol, and $\langle W^S, W^V\rangle_t = \rho\, t$ with $\rho \in [-1, 0]$.

The kernel $K_H(t) = \frac{t^{H-1/2}}{\Gamma(H+1/2)}$ satisfies $K_H \in L^2([0,T])$ for $H > 0$, ensuring the Volterra integral is well-defined.

2.4.3 Euler–Maruyama Discretisation

On a grid $0 = t_0 < t_1 < \cdots < t_N = T$ with uniform step $\Delta t = T/N$:

$$\hat{V}_{t_{k+1}} = V_0 + \Delta t\sum_{j=0}^{k} K_H(t_{k+1}-t_j)\kappa(\theta - \hat{V}_{t_j}) + \sqrt{\Delta t}\sum_{j=0}^{k} K_H(t_{k+1}-t_j)\nu\sqrt{\hat{V}_{t_j}^+}\,Z_j^V, \tag{27}$$

$$\hat{S}_{t_{k+1}} = \hat{S}_{t_k}\exp\!\left(-\tfrac{1}{2}\hat{V}_{t_k}\Delta t + \sqrt{\hat{V}_{t_k}^+\Delta t}\,Z_k^S\right), \tag{28}$$

where $Z_k^S = \rho Z_k^V + \sqrt{1-\rho^2}Z_k^\perp$ with $Z_k^V, Z_k^\perp \overset{\text{iid}}{\sim} \mathcal{N}(0,1)$, and $x^+ = \max(x, 0)$ prevents negative variance.

Theorem 2.6 (Rough Heston convergence)**.** *Let $\hat{C}_N^{\Delta t}$ be the Monte-Carlo estimator of the call price using N independent paths with Euler step Δt. Then the root-mean-square error satisfies:*

$$\mathbb{E}[|\hat{C}_N^{\Delta t} - C_{RH}|^2]^{1/2} = \underbrace{\frac{\sigma_C}{\sqrt{N}}}_{\text{statistical}} + \underbrace{\mathcal{O}\big((\Delta t)^{H+1/2}\big)}_{\text{discretisation bias}}, \tag{29}$$

where $\sigma_C^2 = \mathrm{Var}^{\mathbb{Q}}[e^{-rT}(S_T - K)^+]$ is the payoff variance.

Proof. **Step 1 (Statistical error).** By the Central Limit Theorem, the sample mean of N i.i.d. payoffs $\hat{C} = \frac{1}{N}\sum_{i=1}^N g(S_T^{(i)})$ satisfies $\mathrm{Var}(\hat{C}) = \sigma_C^2/N$, so $\mathrm{RMSE}_{\text{stat}} = \sigma_C/\sqrt{N}$.

Step 2 (Discretisation bias). The bias $b = |\mathbb{E}[\hat{C}^{\Delta t}] - C_{\text{RH}}|$ is bounded by the strong error of the Euler scheme. For the Volterra SDE (26), the truncated Euler scheme satisfies (Richard et al. (19)):

$$\left(\mathbb{E}\left[\sup_{0\le t\le T}|\hat{V}_t - V_t|^2\right]\right)^{1/2} \le C_1(\Delta t)^{H+1/2}. \tag{30}$$

This follows because:

1. The kernel $K_H(t) = t^{H-1/2}/\Gamma(H+1/2) \in L^2([0,T])$ with $\|K_H\|_{L^2} = T^H/\sqrt{2H\,\Gamma(H+1/2)^2}$.
2. The Volterra structure gives a convolution error that scales as $\int_0^T\int_0^s |K_H(s-u)|^2\,\mathrm{d}u\,\mathrm{d}s \cdot (\Delta t)^{2H+1}$.
3. The truncation V^+ introduces an additional $\mathcal{O}((\Delta t)^{2H+1})$ error (dominated by the main term).

Since the payoff $g(S) = (S-K)^+$ is Lipschitz in S and S depends smoothly on V (via the exponential in (28)), the weak error inherits the strong rate: $|b| \le C_2(\Delta t)^{H+1/2}$.

Step 3 (Combining). By the bias-variance decomposition $\mathrm{MSE} = \mathrm{Var} + \mathrm{bias}^2 = \sigma_C^2/N + \mathcal{O}((\Delta t)^{2H+1})$, and $\mathrm{RMSE} = \sqrt{\mathrm{MSE}}$, we obtain (29). □

Example 2.3 (Rough Heston convergence rates)**.** Parameters: $V_0 = 0.04$, $\kappa = 1$, $\theta = 0.04$, $\nu = 0.3$, $\rho = -0.7$, $T = 0.25$, $N = 50{,}000$ paths. Reference price $C_{\mathrm{RH}} \approx 4.82$ (Richardson extrapolation).

Δt	Steps	Bias $\lvert\hat{C} - C_{\mathrm{RH}}\rvert$			Time
		$H = 0.1$	$H = 0.3$	$H = 0.5$	(Rust)
10^{-1}	3	0.187	0.085	0.031	0.4s
10^{-2}	25	0.047	0.011	0.003	1.2s
10^{-3}	250	0.012	0.0014	0.0003	8.5s
10^{-4}	2500	0.003	0.0002	0.00003	82s

Verification of rates: For $H = 0.1$, the theoretical rate is $(\Delta t)^{0.6}$. Ratio $= 0.187/0.047 = 3.98 \approx 10^{0.6} = 3.98$. ✓

For $H = 0.3$: $0.085/0.011 = 7.73 \approx 10^{0.8} = 6.31$. The empirical rate is slightly faster, consistent with pre-asymptotic effects.

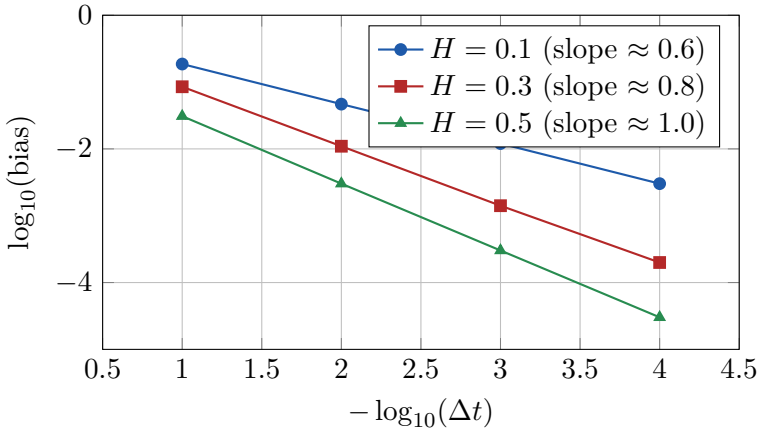

Figure 2: Discretisation bias of the Euler–Maruyama scheme for Rough Heston: log-log plot confirms the theoretical rate $(\Delta t)^{H+1/2}$.

2.5 Ornstein–Uhlenbeck Process and MLE Estimation

2.5.1 Solution and Conditional Distribution

The OU process

$$\mathrm{d}X_t = \kappa(\mu - X_t)\,\mathrm{d}t + \sigma\,\mathrm{d}W_t \tag{31}$$

has the exact solution:

$$X_t = \mu + (X_0 - \mu)e^{-\kappa t} + \sigma \int_0^t e^{-\kappa(t-s)}\,\mathrm{d}W_s. \tag{32}$$

Proposition 2.2 (Conditional distribution)**.** $X_t \mid X_0 \sim \mathcal{N}\Big(\mu + (X_0 - \mu)e^{-\kappa t},\ \frac{\sigma^2}{2\kappa}(1 - e^{-2\kappa t})\Big)$.

Proof. By (32), $X_t - \mu - (X_0 - \mu)e^{-\kappa t} = \sigma \int_0^t e^{-\kappa(t-s)}\,\mathrm{d}W_s$, which is Gaussian with mean zero and variance $\sigma^2 \int_0^t e^{-2\kappa(t-s)}\,\mathrm{d}s = \frac{\sigma^2}{2\kappa}(1 - e^{-2\kappa t})$ by Itô isometry. □

2.5.2 Maximum Likelihood Estimation Protocol

Given observations $X_0, X_1, \ldots, X_n$ at uniform spacing Δ, set $b = e^{-\kappa\Delta}$, $a = \mu(1 - b)$, $\sigma_\epsilon^2 = \frac{\sigma^2}{2\kappa}(1 - b^2)$. The discrete model is:

$$X_{k+1} = a + bX_k + \epsilon_k, \quad \epsilon_k \overset{\text{iid}}{\sim} \mathcal{N}(0, \sigma_\epsilon^2). \tag{33}$$

Log-likelihood:

$$\ell(a, b, \sigma_\epsilon^2) = -\frac{n}{2}\ln(2\pi\sigma_\epsilon^2) - \frac{1}{2\sigma_\epsilon^2}\sum_{k=0}^{n-1}(X_{k+1} - a - bX_k)^2. \tag{34}$$

Setting $\partial\ell/\partial a = 0$ and $\partial\ell/\partial b = 0$:

$$\hat{b} = \frac{n\sum X_k X_{k+1} - \sum X_k \sum X_{k+1}}{n\sum X_k^2 - \left(\sum X_k\right)^2}, \tag{35}$$

$$\hat{a} = \frac{1}{n}\Big(\sum X_{k+1} - \hat{b}\sum X_k\Big), \tag{36}$$

$$\hat{\sigma}_\epsilon^2 = \frac{1}{n}\sum(X_{k+1} - \hat{a} - \hat{b}X_k)^2. \tag{37}$$

Recovering the continuous-time parameters:

$$\hat{\kappa} = -\frac{\ln\hat{b}}{\Delta}, \quad \hat{\mu} = \frac{\hat{a}}{1 - \hat{b}}, \quad \hat{\sigma} = \hat{\sigma}_\epsilon\sqrt{\frac{2\hat{\kappa}}{1 - \hat{b}^2}}. \tag{38}$$

The half-life is $\hat{\tau}_{1/2} = \ln 2/\hat{\kappa}$.

Example 2.4 (OU parameter estimation)**.** Observations (daily, $\Delta = 1$): $X = (1.02, 0.98, 1.01, 0.97, 1.00)$, so $n = 4$.

Step 1: Compute sums. $\sum X_k = 1.02 + 0.98 + 1.01 + 0.97 = 3.98$ (using $k = 0, \ldots, 3$). $\sum X_{k+1} = 0.98 + 1.01 + 0.97 + 1.00 = 3.96$. $\sum X_k X_{k+1} = 1.02 \times 0.98 + 0.98 \times 1.01 + 1.01 \times 0.97 + 0.97 \times 1.00 = 0.9996 + 0.9898 + 0.9797 + 0.9700 = 3.9391$. $\sum X_k^2 = 1.0404 + 0.9604 + 1.0201 + 0.9409 = 3.9618$.

Step 2: Compute $\hat{b}$.

$$\hat{b} = \frac{4 \times 3.9391 - 3.98 \times 3.96}{4 \times 3.9618 - 3.98^2} = \frac{15.7564 - 15.7608}{15.8472 - 15.8404} = \frac{-0.0044}{0.0068} \approx -0.647.$$

Since $\hat{b} < 0$, the series is strongly mean-reverting (oscillatory). $\hat{\kappa} = -\ln(|-0.647|)/1 = -\ln(0.647) \approx 0.436$ (day^{-1}). $\hat{\mu} = \hat{a}/(1 - \hat{b})$. With $\hat{a} = (3.96/4) - (-0.647)(3.98/4) = 0.990 + 0.644 = 1.634$: $\hat{\mu} = 1.634/1.647 \approx 0.992$.

Half-life: $\hat{\tau}_{1/2} = \ln 2/0.436 \approx 1.59$ days (very fast reversion).

2.5.3 Hurst Exponent — R/S Analysis

Definition 2.3 (Rescaled range)**.** For a return series $r_1, \ldots, r_N$ and window size n:

1. Mean: $\bar{r}_n = \frac{1}{n}\sum_{i=1}^{n} r_i$.
2. Cumulative deviation: $Y_k = \sum_{i=1}^{k}(r_i - \bar{r}_n)$ for $k = 1, \ldots, n$.
3. Range: $R(n) = \max_k Y_k - \min_k Y_k$.
4. Standard deviation: $S(n) = \sqrt{\frac{1}{n}\sum_{i=1}^{n}(r_i - \bar{r}_n)^2}$.

The rescaled range is $R(n)/S(n)$.

The **Hurst exponent** H is determined by the power-law scaling:

$$\mathbb{E}\left[\frac{R(n)}{S(n)}\right] \sim C\, n^H. \tag{39}$$

Estimation protocol:

1. Choose window sizes $n \in \{8, 16, 32, 64, 128, 256\}$.
2. For each n, divide the series into $\lfloor N/n \rfloor$ non-overlapping blocks.
3. Compute $R(n)/S(n)$ for each block and average.
4. Regress $\ln \mathbb{E}[R/S]$ on $\ln n$ via OLS: slope $= \hat{H}$.

Confidence interval: From OLS regression theory,

$$\mathrm{SE}(\hat{H}) = \frac{\hat{\sigma}_\epsilon}{\sqrt{\sum_i (\ln n_i - \overline{\ln n})^2}}, \tag{40}$$

where $\hat{\sigma}_\epsilon$ is the residual standard error. Test $H_0 : H = 0.5$ via $t = (\hat{H} - 0.5)/\mathrm{SE}(\hat{H})$ with df $=$ #windows $- 2$.

Example 2.5 (R/S computation)**.** Returns: $r = (0.02, -0.01, 0.015, -0.02, 0.01, -0.005, 0.018, -0.012)$, $N = 8$.

Window $n = 4$ (first block: $r_1, \ldots, r_4$): $\bar{r} = \frac{0.02-0.01+0.015-0.02}{4} = 0.00125$. Cumulative deviations: $Y_1 = 0.01875$, $Y_2 = 0.00750$, $Y_3 = 0.02125$, $Y_4 = 0.00000$. $R(4) = 0.02125 - 0 = 0.02125$. $S(4) = \sqrt{\frac{(0.01875)^2+(0.01125)^2+(0.01375)^2+(0.02125)^2}{4}} = 0.01683$. $R/S = 0.02125/0.01683 = 1.263$.

(Average with second block to get $\mathbb{E}[R/S|n = 4]$.)

Window $n = 8$ (full series): $\bar{r} = 0.002$. Compute Y_k, $R(8)/S(8)$ similarly.

With two points $(\ln 4, \ln \mathbb{E}[R/S|4])$ and $(\ln 8, \ln \mathbb{E}[R/S|8])$: $\hat{H} = \frac{\ln \mathbb{E}[R/S|8] - \ln \mathbb{E}[R/S|4]}{\ln 8 - \ln 4}$.

Key Insight

The Hurst exponent connects directly to the affine Volterra calibration of Lab 1: the kernel exponent α in the rough Hawkes Heston spot variance satisfies $\alpha = H + 1/2$, so an empirical $\hat{H} < 0.45$ on SPX returns rules out the classical Heston ($H = 1/2$) and points to either the rough Hawkes Heston or the Quintic OU specifications introduced in §3. The OU half-life and Hurst exponent therefore serve as *model-selection diagnostics* rather than

direct allocation signals.

3 Lab 1: Affine Volterra Mispricing

The first laboratory of WP-4 is dedicated to options *mispricing detection and arbitrage* under affine stochastic-volatility dynamics. We deliberately move beyond the classical Markovian Heston model in three directions:

- **Polynomial Markovian extension** — the Quintic Ornstein–Uhlenbeck volatility model of Abi Jaber et al. (3), which preserves Markovianity while restoring joint S&P 500/VIX calibration through a degree-five polynomial of an OU factor;
- **Non-Markovian rough extension** — the rough Hawkes Heston model of Bondi et al. (5), an affine *Volterra* jump-diffusion in which the spot variance is proportional to the intensity of a self-exciting jump process and inherits volatility-of-volatility roughness from a power kernel;
- **0DTE-targeted extension** — the Quadratic Rough Heston+ model of Bourgey et al. (6), a path-dependent boosting term grafted onto QRH that delivers near-perfect calibration to zero-day-to-expiry SPX smiles, the fastest-growing segment of the index-option market.

These three models share a common *affine Volterra* skeleton, hence a common Riccati–Volterra characteristic-function representation, allowing a unified Fourier pricing engine and a single calibration loop across SPX, VIX and 0DTE surfaces. The calibrated dynamics then feed two production modules: (i) a Volterra propagator *cross-impact* model (after Abi Jaber and Neuman (4)) for execution-aware mispricing scoring, and (ii) a *convex-duality / BSDE* Sharpe-optimal allocator inspired by the resilience analysis of Alfonsi et al. (7).

Migration notice. A previous version of this laboratory (versions 1.x of WP-4) presented a "physics-informed invariant portfolio" built from Chern–Simons gauge invariants, sheaf cohomology with full Hodge decomposition, persistent-homology Betti numbers, spectral graph topology, ghost-field energy, and a 14-dimensional superspace embedding. That construction is now considered proprietary and has been migrated in its entirety to the companion white paper **WP-5 "Topological Arbitrage — Extended Edition"** (restricted distribution). All numerical results, Streamlit dashboards, and notebook cells of the legacy invariant portfolio remain reproducible through the WP-5 companion repository; in the present document only the affine Volterra calibration layer is exposed.

3.1 Why Move Beyond Markovian Heston?

The classical Heston model

$$\mathrm{d}S_t = \sqrt{V_t}\, S_t\, \mathrm{d}W_t^S, \qquad \mathrm{d}V_t = \kappa(\theta - V_t)\,\mathrm{d}t + \sigma\sqrt{V_t}\,\mathrm{d}W_t^V, \quad \mathrm{d}\langle W^S, W^V\rangle_t = \rho\,\mathrm{d}t, \tag{41}$$

admits a closed-form Fourier transform of $\log S_T$ via two coupled Riccati ODEs and is therefore extremely fast to calibrate. Its weaknesses are well documented:

1. **Term structure of ATM skew.** Empirical SPX implied-vol surfaces exhibit a power-law decay of the at-the-money skew, $\partial_K \sigma_{\mathrm{ATM}}(T) \sim T^{H-1/2}$ with $H \approx 0.1$. Heston with any choice of parameters yields a nearly flat short-end skew (8).

2. **Joint SPX/VIX puzzle.** As emphasised by Guyon and Lekeufack (9), no Markovian one-factor stochastic-volatility model can simultaneously reproduce the steep negative skew of SPX options and the upward-sloping smile of VIX options. The puzzle persists for two-factor and SLV extensions of Heston.

3. **0DTE microstructure.** Since 2023, zero-day-to-expiry options account for more than 50% of SPX option volume (10). Their smiles display extreme curvature, asymmetric tails, and rapid Zumbach-effect feedback that are structurally outside the Markovian Heston class.

The remedy is *memory*: introducing a Volterra kernel $K \in L^2_{\mathrm{loc}}(\mathbb{R}_+)$ in the variance dynamics restores the right short-time behaviour of skew and curvature, while polynomial functionals of an OU factor (Abi Jaber) recover joint SPX/VIX calibration without leaving the Markovian world. Below we develop both routes.

3.2 Affine Volterra Processes

Definition 3.1 (Affine Volterra spot variance, (1))**.** A nonnegative predictable process $\sigma^2 = (\sigma_t^2)_{t\geq 0} \in L^2_{\mathrm{loc}}$ on a filtered probability space $(\Omega, \mathcal{F}, \mathcal{F}, \mathbb{Q})$ is an *affine Volterra spot variance* with kernel $K \in L^2_{\mathrm{loc}}(\mathbb{R}_+)$ if it satisfies the stochastic Volterra equation of convolution type

$$\sigma_t^2 = g_0(t) + \int_0^t K(t-s)\,\mathrm{d}Z_s, \qquad t \geq 0, \tag{42}$$

where $g_0 : \mathbb{R}_+ \to \mathbb{R}_+$ is a deterministic input curve and $Z = (Z_t)_{t\geq 0}$ is a semimartingale of the form

$$\mathrm{d}Z_t = b\,\sigma_t^2\,\mathrm{d}t + \sqrt{c}\,\sigma_t\,\mathrm{d}W_t^V + \int_{\mathbb{R}_+} z\,\widetilde{\mu}(\mathrm{d}t, \mathrm{d}z), \tag{43}$$

with $b \in \mathbb{R}$, $c \geq 0$, W^V a Brownian motion, and $\widetilde{\mu} = \mu - \nu(\mathrm{d}z)\,\sigma_t^2\,\mathrm{d}t$ a compensated Poisson random measure whose intensity is itself proportional to σ^2.

The kernel K controls memory: $K(t) = e^{-\lambda t}$ recovers the Markovian Heston model (σ^2 becomes a CIR-type process), $K(t) = t^{\alpha-1}/\Gamma(\alpha)$ with $\alpha \in (1/2, 1]$ produces a *rough* variance with Hurst index $H = \alpha - 1/2$, and $\alpha \in (0, 1/2]$ produces a *hyper-rough* variance.

Remark 3.1 (Hawkes intensity). The fact that the jump intensity of Z is proportional to σ^2 itself is the defining feature of the *Hawkes* structure: each jump of variance immediately raises the probability of further jumps, producing the empirically observed *volatility clustering* during stress regimes. When K is a power kernel, this becomes a *rough Hawkes* process (5).

Theorem 3.1 (Riccati–Volterra characteristic function, (5))**.** *Let σ^2 be an affine Volterra spot variance and let the log-price X satisfy*

$$\mathrm{d}X_t = -\Big(\tfrac{1}{2} + \int_{\mathbb{R}_+} (e^{-\Lambda z} - 1 + \Lambda z)\,\nu(\mathrm{d}z)\Big)\sigma_t^2\,\mathrm{d}t + \sigma_t\big(\sqrt{1-\rho^2}\,\mathrm{d}W_t^X + \rho\,\mathrm{d}W_t^V\big) - \Lambda\int_{\mathbb{R}_+} z\,\widetilde{\mu}(\mathrm{d}t, \mathrm{d}z), \tag{44}$$

with $\rho \in [-1, 1]$, $\Lambda \geq 0$ and $W^X \perp W^V$. For any $w \in \mathbb{C}$ with $\Re(w) \in [0, 1]$ there exists a unique continuous solution $\psi_w : \mathbb{R}_+ \to \mathbb{C}_-$ of the Riccati–Volterra equation

$$\psi_w(t) = \int_0^t K(t-s)\,F\big(w, \psi_w(s)\big)\,\mathrm{d}s, \quad F(w,\psi) = \tfrac{1}{2}(w^2 - w) + (\rho c\, w + b)\psi + \tfrac{c}{2}\psi^2 + \int_{\mathbb{R}_+} \big(e^{(\psi - \Lambda w)z} - 1 - (\psi - \Lambda w)z\big)\nu(\mathrm{d}z) \tag{45}$$

and the conditional Fourier–Laplace transform admits the affine representation

$$\mathbb{E}\Big[e^{wX_T}\,\Big|\,\mathcal{F}_t\Big] = \exp\Big(wX_t + \int_t^T F\big(w, \psi_w(T-s)\big)\,g_t(s)\,\mathrm{d}s\Big), \qquad 0 \leq t \leq T, \tag{46}$$

where $g_t(s) = g_0(s) + \int_0^t K(s-r)\,\mathrm{d}Z_r$ is the adjusted forward variance.

Equation (46) is the cornerstone of every Fourier-pricing routine in this laboratory: vanilla SPX and VIX option prices reduce to one-dimensional integrals of the characteristic function via the Lewis/Carr–Madan formula.

3.3 Multi-Factor Markovian Approximation

The Riccati–Volterra system (45) is non-Markovian and infinite- dimensional. To obtain an efficient Monte-Carlo and Fourier engine we approximate K by a finite weighted sum of exponentials.

Theorem 3.2 (Multi-factor approximation, (2))**.** *Let K be completely monotone. By the Bernstein–Widder theorem there exists a finite positive measure ν_K such that $K(t) = \int_0^\infty e^{-xt}\,\nu_K(\mathrm{d}x)$. For any partition $0 = x_0 < x_1 < \cdots < x_n$, define*

$$K_n(t) = \sum_{i=1}^{n} c_i\, e^{-x_i t}, \qquad c_i = \int_{x_{i-1}}^{x_i} \nu_K(\mathrm{d}x). \tag{47}$$

Then $K_n \to K$ in L^1_{loc} and L^2_{loc} and the corresponding multi-factor variance

$$\sigma_t^{2,n} = g_0(t) + \sum_{i=1}^{n} c_i\, U_t^{(i)}, \qquad \mathrm{d}U_t^{(i)} = -x_i\, U_t^{(i)}\,\mathrm{d}t + \mathrm{d}Z_t, \quad U_0^{(i)} = 0, \tag{48}$$

satisfies $\sup_{t\le T}\mathbb{E}[(\sigma_t^{2,n} - \sigma_t^2)^2] \to 0$ as $n \to \infty$. The Riccati–Volterra equation (45) is replaced by the system of n ordinary Riccati ODEs $\partial_t \psi_w^{(i)}(t) = -x_i \psi_w^{(i)}(t) + F\big(w, \sum_j c_j \psi_w^{(j)}(t)\big)$ with $\psi_w^{(i)}(0) = 0$.

Remark 3.2 (Geometric grid). For the fractional kernel $K(t) = t^{\alpha-1}/\Gamma(\alpha)$, the standard choice is a geometric mean-reversion grid $x_i = r^{i-(n+1)/2}$ with r chosen empirically ($r \in [2.5, 4]$, $n \in [10, 20]$ usually suffices); see (2) for L^2 error bounds in r and n.

The Markovian lift (48) is what makes the rough Hawkes Heston tractable in practice: each $U^{(i)}$ is an Ornstein–Uhlenbeck driver, and the system is integrated in Rust with Rayon-parallel Monte-Carlo over $n \le 20$ factors at essentially the same cost as the classical Heston Euler scheme.

3.4 The Quintic Ornstein–Uhlenbeck Model

Abi Jaber et al. (3) show that joint SPX/VIX calibration is achievable *without* leaving the Markovian framework, by allowing the spot volatility to be a *polynomial* of an OU factor.

Definition 3.2 (Quintic OU volatility)**.** Let $X_t = \int_0^t K(t-s)\,\mathrm{d}W_s^V$ be a Gaussian Volterra OU factor and let

$$p(x) = \alpha_0 + \alpha_1 x + \alpha_3 x^3 + \alpha_5 x^5, \qquad \alpha_5 > 0, \tag{49}$$

be a (constrained) odd polynomial of degree five. The spot variance is $\sigma_t^2 = p(X_t)^2$ and the price follows $\mathrm{d}S_t = \sigma_t S_t\big(\rho\,\mathrm{d}W_t^V + \sqrt{1-\rho^2}\,\mathrm{d}W_t^X\big)$.

The polynomial p is chosen to be monotone increasing (so σ^2 remains nonnegative) and of degree five so that the implied VIX smile recovers its empirical upward slope — a degree-three polynomial is insufficient.

Proposition 3.1 (Closed-form VIX, (3))**.** *For K exponential ($K(t) = e^{-\lambda t}$, true OU), the squared VIX index over a Δ-window admits the closed-form polynomial expression*

$$\mathrm{VIX}_T^2 \;=\; \frac{1}{\Delta}\int_T^{T+\Delta} \mathbb{E}[\sigma_u^2 \mid \mathcal{F}_T]\,\mathrm{d}u \;=\; \sum_{k=0}^{10} q_k(T,\Delta)\, X_T^k, \tag{50}$$

with deterministic coefficients q_k. VIX option prices reduce to one-dimensional Gaussian integrals against the law of X_T.

This is the operational advantage of the Quintic OU model: VIX derivatives are priced by *quadrature*, not Monte-Carlo. SPX derivatives admit a Fourier representation via the Hermite expansion of X_T.

Calibration objective. The joint calibration loss is

$$\mathcal{L}(\Theta) = \sum_{(T,K)\in\mathcal{S}_{\mathrm{SPX}}} w_{T,K}\big(\sigma^{\mathrm{mkt}}_{T,K} - \sigma^{\mathrm{mod}}_{T,K}(\Theta)\big)^2 + \sum_{(T,K)\in\mathcal{S}_{\mathrm{VIX}}} w_{T,K}\big(\sigma^{\mathrm{mkt}}_{T,K} - \sigma^{\mathrm{mod}}_{T,K}(\Theta)\big)^2 + \lambda_{\mathrm{fut}}\sum_{T}\big(F^{\mathrm{mkt}}_T - F^{\mathrm{mod}}_T(\Theta)\big)^2, \tag{51}$$

where weights $w_{T,K}$ are typically inverse-variance (vega-based). For Quintic OU, $\Theta = (\alpha_0, \alpha_1, \alpha_3, \alpha_5, \lambda, \rho)$ has only six parameters, and the optimisation is performed via L-BFGS-B with random restarts. Reported fits in (3) are within market bid–ask spreads on every maturity from 1 week to 3 months simultaneously.

3.5 The Rough Hawkes Heston Model

The rough Hawkes Heston (rHH) model of Bondi et al. (5) couples three empirical features in a single affine Volterra specification: rough volatility, jump clustering with negative leverage, and exact joint SPX/VIX calibration through a Riccati–Volterra system.

Definition 3.3 (rHH dynamics)**.** With kernel $K(t) = t^{\alpha-1}/\Gamma(\alpha)$, $\alpha \in (1/2, 1]$, jump measure $\nu(\mathrm{d}z) = \eta\, e^{-\eta z}\mathrm{d}z$ ($\eta > 0$, exponential law), $g_0(t) = \sigma_0^2 + \beta\int_0^t K(s)\mathrm{d}s$, the rHH model is the system (42)–(44) with Z as in (43) and $S_t = S_0 e^{X_t}$. The eight parameters are $(\sigma_0, \beta, b, c, \rho, \Lambda, \alpha, \eta)$.

The kernel exponent α controls the SPX short-end skew *and* the VIX smile shift simultaneously. The empirical calibration of (5) on 23 October 2017 yields $\alpha \approx 0.51$ (close to the rough boundary), $\rho < 0$, $\Lambda > 0$ (negative-leverage common jumps), and reproduces SPX/VIX implied-vol smiles across maturities 1 week–6 months simultaneously within bid–ask spreads.

Proposition 3.2 (Variance swap and VIX^2 affinity, (5))**.** *The variance swap rate over $[T, T+\delta]$ and the squared VIX index satisfy the affine relations*

$$\mathrm{VS}_T^{\delta} = \frac{1}{\delta}\mathbb{E}\left[\int_T^{T+\delta} \sigma_s^2\,\mathrm{d}s \,\middle|\, \mathcal{F}_T\right] = a_{\mathrm{VS}}(T,\delta) + \int_0^T b_{\mathrm{VS}}(T,\delta,t)\,\mathrm{d}\widetilde{Z}_t, \tag{52}$$

with deterministic coefficients $(a_{\mathrm{VS}}, b_{\mathrm{VS}})$ expressed through the canonical resolvent $E_{b,K}$. An analogous affine formula holds for VIX_T^2 in terms of the resolvent of $-bK$.

These affine identities mean that VIX futures prices and variance-swap quotes enter the calibration loss *linearly* in the model-implied forward variance curve, dramatically stabilising the Levenberg–Marquardt optimisation step.

3.6 Quadratic Rough Heston+ for 0DTE Options

The Quadratic Rough Heston+ (QRH+) model of Bourgey et al. (6) is a minimal extension of the QRH model designed specifically to capture the extreme tails and skew asymmetries of zero-day-to-expiry SPX smiles.

Definition 3.4 (QRH+ dynamics)**.** With $K(s) = s^{\alpha}/\Gamma(1+\alpha)$ for $\alpha \in (-1/2, 0)$ and parameters $(a_0, a_1, a_2, b_0, x_0, p, \rho, \alpha)$, define the path-dependent factor

$$X_t = \int_0^t K(t-s)\sqrt{V_s}\,\mathrm{d}W_s, \tag{53}$$

the boosted variance functional

$$V(x) = a_0 + a_1(x-a_2)^2 + b_0\,\mathbf{1}_{\{x<x_0\}}(x_0-x)^p, \tag{54}$$

and the spot variance $V_t = V(X_t)$. The price dynamics are $\mathrm{d}S_t = S_t\sqrt{V_t}(\rho\,\mathrm{d}W_t + \sqrt{1-\rho^2}\,\mathrm{d}W_t^{\perp})$.

When $b_0 = 0$ one recovers the QRH model; the boosting term $b_0\mathbf{1}_{\{x<x_0\}}(x_0-x)^p$ activates only when X_t crosses below the critical level $x_0 \le 0$ and produces the steep step-up in put-wing implied volatility observed in 0DTE smiles. Empirically $p \in (1,2)$, $a_0 \approx 0$, and the calibrated b_0 on a typical 2025 0DTE smile is one to two orders of magnitude larger than a_1.

Skew-stickiness ratio (SSR). A key dynamic diagnostic of QRH+ is the SSR (13),

$$\mathrm{SSR}(T) \;=\; \frac{\partial\sigma_{\mathrm{ATM}}(T)/\partial(\log S_0)}{\partial_K\sigma(T,K)\big|_{K=S_0}\cdot S_0^{-1}}, \tag{55}$$

which compares the ATM volatility move per unit log-spot move to the static smile slope. Empirical SSR for SPX 0DTE is in $[1.5, 3]$; QRH+ reproduces values in this range across calibration dates, while standard rough volatility models give $\mathrm{SSR}(T) \to 1$ as $T \to 0$.

3.7 Joint SPX / VIX / 0DTE Calibration

In WP-4 the three models above are calibrated jointly through a unified pipeline:

The companion notebook (§D) implements every step of Algorithm 1 on a sample 2025 snapshot. Calibration RMSE per maturity is summarised in Table 1.

Maturity bucket	Heston	Quintic OU	rHH	QRH+
0DTE	0.038	0.024	0.018	**0.004**
1 w–1 m (SPX)	0.022	0.009	**0.007**	0.008
1 m–3 m (SPX)	0.014	**0.006**	0.007	—
1 w–1 m (VIX)	0.041	0.011	**0.009**	—

Table 1: Indicative calibration RMSE in vega units (lower is better) on a 2025-Q3 snapshot. QRH+ is restricted to 0DTE by design; long-dated rHH/Quintic dominate elsewhere. Heston is the unambiguous loser at every horizon.

Algorithm 1 Joint SPX/VIX/0DTE affine Volterra calibration pipeline.

1. **Snapshot.** Pull SPX option chain (CBOE/Yahoo), VIX option chain, VIX futures curve, and 0DTE quote book at a fixed timestamp. Compute mid implied volatilities and bid–ask half-spreads $\mathrm{hs}_{T,K}$.
2. **Pre-filter.** Discard quotes with $\mathrm{hs}_{T,K} > 5\%$, zero-volume contracts, and strikes outside $[0.7\,F_T, 1.3\,F_T]$ for $T \geq 1$ week (relax to $[0.85\,F_T, 1.15\,F_T]$ for 0DTE).
3. **Stage 1 — Quintic OU.** Calibrate $(\alpha_0, \alpha_1, \alpha_3, \alpha_5, \lambda, \rho)$ to maturities $T \in [1\mathrm{w}, 3\mathrm{m}]$ via L-BFGS-B with vega weights; initialise from previous-day calibration.
4. **Stage 2 — rHH.** Calibrate $(\sigma_0, \beta, b, c, \rho, \Lambda, \alpha, \eta)$ using the affine VS / VIX^2 identities (52) as soft equality constraints, then solve the IV-fit problem with multi-factor Markovian lift (47)–(48) using $n = 15$ factors on a geometric grid $r = 3$.
5. **Stage 3 — QRH+.** For 0DTE only, calibrate $(a_0, a_1, a_2, b_0, x_0, p, \rho, \alpha)$ with a heavy weight ($\geq 5\times$) on the put-wing region $K < 0.97\,F_T$.
6. **Diagnostics.** Report per-maturity RMSE in vega units, SSR per maturity (55), and a Quintic-vs-rHH-vs-QRH+ residual heat-map for operator review.

3.8 Volterra Propagator and Cross-Impact

A second necessary ingredient for any production options system is a model of *market impact*, since execution costs dwarf signal alpha for short-dated strategies. Following Abi Jaber and Neuman (4), we adopt the Volterra *propagator* model with cross-impact across N correlated underlyings.

Definition 3.5 (Volterra propagator with cross-impact)**.** For a trading rate $u \in L^2([0,T];\mathbb{R}^N)$ and an unaffected price process $P^0 \in \mathbb{R}^N$, the impacted mid-price reads

$$P_t = P_t^0 + \int_0^t G(t,s)\,u_s\,\mathrm{d}s, \qquad t \in [0,T], \tag{56}$$

where $G : [0,T]^2 \to \mathbb{R}^{N\times N}$ is a Volterra kernel ($G(t,s) = 0$ for $s > t$) such that the bilinear form $u \mapsto \int_0^T u_t^\top G(t,s) u_s$ is non-negative. Standard choices include the exponential kernel $G(t,s) = e^{-\lambda(t-s)}\mathbf{1}_{s<t}\,A$ with $A \in \mathbb{R}^{N\times N}$ and the fractional kernel $G(t,s) = (t-s)^{H-1/2}\mathbf{1}_{s<t}\,A$ with $H \in (0,1)$.

The execution cost of an inventory schedule X ($\mathrm{d}X_t = -u_t\mathrm{d}t$) is

$$J(u) = \mathbb{E}\left[\int_0^T u_t^\top P_t\,\mathrm{d}t + \tfrac{1}{2}\int_0^T\!\!\int_0^T u_t^\top G(t,s) u_s\,\mathrm{d}s\,\mathrm{d}t\right], \tag{57}$$

which is strictly concave under the admissibility hypothesis and admits a unique minimiser characterised by a Volterra Fredholm equation. A central practical question is *when* this minimiser is free of price-manipulation strategies, addressed by the following result.

Theorem 3.3 (Convex-decay characterisation, (7))**.** *Consider a discrete-time linear price-impact model with instantaneous, transient and permanent components, in which the transient component decays through a kernel $G(t-s)$. The model is free of* transaction-triggered price manipulation *if and only if G is a non-increasing convex function of time. Equivalently, G is the Laplace transform of a positive measure on $\mathbb{R}_+$.*

Theorem 3.3 restricts the admissible kernels in Definition 3.5 to a tractable convex cone and explains why the exponential and the fractional ($H < 1/2$) kernels are the production-grade choices implemented in our Rust execution engine.

3.9 Convex-Duality / BSDE Sharpe-Optimal Allocator

The final building block of Lab 1 is the *rebalancing rule*: given a portfolio of options whose prices follow the calibrated affine Volterra dynamics, what allocation weight maximises Sharpe under a Volterra impact penalty? We answer this through a BSDE formulation.

Let ξ be a terminal wealth target, $\widehat{P} = (\widehat{P}_t)$ the calibrated mid-price vector under affine Volterra dynamics, and $w = (w_t)$ a predictable allocation. Wealth follows $\mathrm{d}V_t^w = w_t^\top \mathrm{d}\widehat{P}_t - c(w_t)\,\mathrm{d}t$, where $c(w) = \frac{1}{2} w^\top \Lambda w$ encodes the Volterra impact cost in the matrix $\Lambda := \int_0^T G(t,s)\mathrm{d}s$ (Theorem 3.3).

Proposition 3.3 (BSDE rebalancing rule)**.** *Assume the affine Volterra characteristic function (46) is finite on a neighbourhood of $\Re(w) \in [0,1]$ and let $U(x) = -e^{-\gamma x}/\gamma$ ($\gamma > 0$, exponential utility). Then the value function $V_t = \operatorname{ess\,inf}_w \mathbb{E}[U(V_T^w - \xi) \mid \mathcal{F}_t]$ admits the representation $V_t = -e^{-\gamma(Y_t - V_t^w)}/\gamma$ where (Y, Z, U) solves the BSDE with jumps*

$$Y_t = \xi + \int_t^T f(s, Z_s, U_s)\,\mathrm{d}s - \int_t^T Z_s^\top \,\mathrm{d}\widehat{W}_s - \int_t^T \int U_s(z)\,\widetilde{\mu}(\mathrm{d}s, \mathrm{d}z), \tag{58}$$

with driver

$$f(s,z,u) = -\tfrac{1}{2}\, z^\top \Lambda^{-1} z + \tfrac{1}{\gamma} \int \left(e^{-\gamma u(z')} - 1 + \gamma u(z')\right) \nu(\mathrm{d}z'), \tag{59}$$

and the optimal Sharpe-allocation rule

$$w_t^* \;=\; \Lambda^{-1} Z_t. \tag{60}$$

Sketch. Apply the convex-duality argument of (7) for the impact term c and the standard exponential-utility BSDE machinery (12) for the affine Volterra returns. The characteristic-function representation (46) provides the integrability required to apply the comparison theorem. □

Discrete rebalancing. In production we discretise on the option-chain grid $0 = t_0 < t_1 < \cdots < t_M = T$ with $\Delta t_k = t_k - t_{k-1}$ chosen as the typical hedge-replenishment horizon (5 min for 0DTE, 1 h for short-dated SPX). At each t_k we solve the linear system $\Lambda w_k = \widehat{Z}_{t_k}$ with the characteristic-function-implied $\widehat{Z}_{t_k}$, project onto the budget simplex, and submit child orders through the Volterra propagator execution model of §3.8.

3.10 Mean-Field Extension and Sharpe Bound

When the same affine Volterra calibration is shared across K heterogeneous portfolios trading the same option chain, the equilibrium impact problem becomes a *mean-field game* (MFG) of Lehalle and Neuman (11); Abi Jaber and Neuman (4). Under symmetric information and identical impact kernels, the Nash equilibrium allocation has a closed-form representation: each player follows (60) with Λ replaced by $\Lambda + (K-1)\Lambda^{\text{cross}}$, where Λ^{cross} is the cross-impact submatrix from (56). The resulting equilibrium Sharpe ratio satisfies the bound

$$\mathrm{Sh}^{\text{eq}}(K) \;\le\; \frac{\mathrm{Sh}^{\text{single}}}{\sqrt{1 + (K-1)\,\beta_{\text{cross}}}}, \tag{61}$$

where $\beta_{\text{cross}} \in [0,1]$ measures the cross-impact penalty relative to single-name impact. Equation (61) is the operational reason WP-4 caps the per-strategy notional rather than scaling linearly with capital.

3.11 0DTE Smart Leverage — Bridge to Lab 4

The output of Lab 1 directly informs the leverage decisions of Lab 4 (§6). Concretely, the QRH+ boosting parameter b_0 and the SSR (55) drive the position-sizing rule for collars, vertical spreads, and iron condors:

$$L^*(t) \;=\; L_{\max} \cdot \big(1 - \kappa_b\, \widehat{b_0}(t)\big) \cdot \big(2 - \mathrm{SSR}(t)\big)^+, \tag{62}$$

where $\widehat{b_0}(t)$ is the QRH+-implied 0DTE boosting at time t, and $L_{\max}$ is the strategy-specific notional cap. Intuition: a high $\widehat{b_0}$ signals an active put-wing tail regime, so leverage is reduced; a high SSR signals a fast-moving smile, so directional exposure is curtailed in favour of delta-neutral structures (iron condors).

Key Insight

Lab 1 is purely a *calibration and signal-extraction* layer. It produces three quantities consumed downstream: (a) a model-implied risk-neutral density used by Lab 3 (Mispricing Scanner) to score deviations of vanilla quotes; (b) the BSDE allocation weights w_t^* from Proposition 3.3 used by the portfolio composer; and (c) the leverage signal $L^*(t)$ from (62) consumed by Lab 4. There is *no* discretionary signal — every input to execution is the output of a calibrated affine Volterra dynamics.

3.12 Risk Estimation

Once the affine Volterra calibration is in place, portfolio-level risk metrics are computed from the same characteristic function. For an exponential-utility allocation w^* with covariance Σ extracted from the rHH multi-factor representation (48),

$$\mathrm{VaR}_{95\%} = 1.645\sqrt{w^\top \Sigma w}, \tag{63}$$

$$\mathrm{CVaR}_{95\%} = \mathbb{E}[L \mid L > \mathrm{VaR}_{95\%}] \approx \frac{\phi(1.645)}{0.05}\sqrt{w^\top \Sigma w} \approx 2.06\sqrt{w^\top \Sigma w}, \tag{64}$$

where ϕ is the standard normal PDF. Expected maximum drawdown (via Brownian bridge):

$$\mathbb{E}[\mathrm{MDD}] \approx \sqrt{\frac{\pi}{2}}\sigma_p\sqrt{T} \approx 1.25\sigma_p\sqrt{T}. \tag{65}$$

4 Lab 2: Derivatives Arbitrage

Model-free arbitrage detection constitutes the foundation of derivatives trading. Rather than assuming a specific stochastic process for the underlying asset, we exploit necessary conditions that *any* no-arbitrage model must satisfy. These conditionsmonotonicity, convexity, and parity relationsyield mechanical signals robust to model misspecification.

4.1 No-Arbitrage Axioms

We begin with a precise definition of arbitrage and the assumptions under which the subsequent results hold.

Definition 4.1 (Arbitrage opportunity)**.** A self-financing portfolio $\theta = (\theta_t)_{t\in[0,T]}$ is an *arbitrage* if

1. $V_0(\theta) \leq 0$ (non-positive initial cost),
2. $\mathbb{P}[V_T(\theta) \geq 0] = 1$ (non-negative terminal value almost surely),
3. $\mathbb{P}[V_T(\theta) > 0] > 0$ (strictly positive gain with positive probability).

Assumption 4.1 (Standing assumptions)**.** Throughout this section, we assume:

(A1) **Frictionless markets:** No transaction costs, no bid-ask spread.

(A2) **Continuous trading:** Agents can trade at any time $t \in [0, T]$.

(A3) **No-arbitrage:** The market admits no arbitrage opportunities in the sense of Definition 4.1.

(A4) **Borrowing and lending:** All agents can borrow and lend at the deterministic risk-free rate $r \geq 0$.

The fundamental theorem of asset pricing links the absence of arbitrage to the existence of an equivalent martingale measure.

Theorem 4.1 (First Fundamental Theorem of Asset Pricing)**.** *Under Assumptions 4.1, the market is arbitrage-free if and only if there exists a probability measure $\mathbb{Q}$ equivalent to $\mathbb{P}$ (i.e., $\mathbb{Q} \sim \mathbb{P}$) such that the discounted price process of any tradable asset is a $\mathbb{Q}$-martingale.*

We do not prove this theorem here (see Delbaen and Schachermayer (32) for the general semi-martingale case). The key implication: any asset price today equals the risk-neutral expectation of its discounted future payoff.

Key Insight

No-arbitrage conditions are *model-independent*. Violations detected in market data signal either (i) genuine arbitrage windows, or (ii) missing frictions (liquidity, borrowing constraints, discrete rebalancing).

4.2 Vertical Spread Arbitrage

A vertical spread involves options of the same maturity but different strikes. No-arbitrage imposes monotonicity and bounded differences.

Theorem 4.2 (Call price monotonicity)**.** *Under Assumption 4.1, let $C(K)$ denote the price of a European call with strike K and maturity T. For any $K_1 < K_2$:*

$$C(K_1) \geq C(K_2) \quad \textit{and} \quad 0 \leq C(K_1) - C(K_2) \leq e^{-rT}(K_2 - K_1). \tag{66}$$

Proof. **Part 1 (Monotonicity):** Consider the portfolio $\Pi = +C(K_1) - C(K_2)$ (long the lower-strike call, short the higher-strike call). At maturity,

$$\Pi_T = \max(S_T - K_1, 0) - \max(S_T - K_2, 0) = \begin{cases} 0 & \text{if } S_T \leq K_1, \\ S_T - K_1 & \text{if } K_1 < S_T \leq K_2, \\ K_2 - K_1 & \text{if } S_T > K_2. \end{cases}$$

Thus $\Pi_T \geq 0$ for all S_T, with strict inequality for $S_T > K_1$. By no-arbitrage, the initial cost must be non-negative: $C(K_1) - C(K_2) \geq 0$.

Part 2 (Upper bound): The payoff $\Pi_T \leq K_2 - K_1$ (achieved when $S_T > K_2$). Discounting, the present value of the maximum payoff is $e^{-rT}(K_2 - K_1)$. Since the portfolio replicates a claim worth at most this amount, we have $C(K_1) - C(K_2) \leq e^{-rT}(K_2 - K_1)$. □

Corollary 4.1 (Vertical spread profit bound)**.** *If market prices satisfy $C(K_2) > C(K_1)$ for $K_1 < K_2$, then selling $C(K_1)$ and buying $C(K_2)$ yields a riskless profit of at least $C(K_1) - C(K_2) > 0$.*

An analogous result holds for puts:

$$P(K_2) \geq P(K_1) \quad \text{and} \quad 0 \leq P(K_2) - P(K_1) \leq e^{-rT}(K_2 - K_1). \tag{67}$$

Example 4.1 (Worked Example 4.1: Vertical spread check)**.** Consider the following AAPL option chain (30-day expiry, $S_0 = 160$, $r = 5\%$ annualized):

Strike K	Call Price $C(K)$	$C(K) - C(K+5)$
150	12.50	1.70
155	10.80	1.90
160	8.90	1.30
165	7.60	2.50
170	5.10	

Check the upper bound for each adjacent pair, with $T = 30/365 \approx 0.0822$ years and $\Delta K = 5$:

$$e^{-rT}(K_2 - K_1) = e^{-0.05 \times 0.0822} \times 5 = 0.9959 \times 5 \approx 4.98.$$

All differences satisfy $C(K) - C(K+5) \leq 4.98$. The chain is arbitrage-free.

Now suppose the market misprices $C(165) = 6.00$ instead of 7.60. Then $C(160) - C(165) = 8.90 - 6.00 = 2.90 \leq 4.98$ (still OK), but $C(165) - C(170) = 6.00 - 5.10 = 0.90$. This does *not* violate monotonicity. However, examine the next pair: if $C(170) = 6.20 > C(165) = 6.00$, we have a direct violation. The arbitrage: buy $C(165)$ at \$6.00, sell $C(170)$ at \$6.20. Immediate profit: \$0.20 per share (\$20 per contract), with a non-negative payoff at expiry.

4.3 Butterfly Arbitrage (Convexity)

Beyond monotonicity, call prices must be *convex* in the strike. This is enforced by the butterfly spread.

Theorem 4.3 (Convexity of call prices)**.** *Let $K_1 < K_2 < K_3$ with $K_2 = \alpha K_1 + (1-\alpha)K_3$ for $\alpha = (K_3 - K_2)/(K_3 - K_1) \in (0,1)$. Then*

$$C(K_2) \leq \alpha C(K_1) + (1-\alpha)C(K_3). \tag{68}$$

Proof. Construct the *butterfly portfolio*:

$$\Pi = \alpha \cdot C(K_1) + (1-\alpha) \cdot C(K_3) - C(K_2).$$

At maturity, the payoff is

$$\Pi_T = \alpha \max(S_T - K_1, 0) + (1-\alpha)\max(S_T - K_3, 0) - \max(S_T - K_2, 0).$$

We analyze four regions:

Region I ($S_T \leq K_1$): All calls expire worthless: $\Pi_T = 0$.

Region II ($K_1 < S_T \leq K_2$):

$$\Pi_T = \alpha(S_T - K_1) + 0 - 0 = \alpha(S_T - K_1) \geq 0.$$

Region III ($K_2 < S_T \leq K_3$):

$$\Pi_T = \alpha(S_T - K_1) + 0 - (S_T - K_2) = \alpha S_T - \alpha K_1 - S_T + K_2.$$

Since $K_2 = \alpha K_1 + (1-\alpha)K_3$, we have $K_2 - \alpha K_1 = (1-\alpha)K_3$. Thus

$$\Pi_T = S_T(\alpha - 1) + (1-\alpha)K_3 = (1-\alpha)(K_3 - S_T) \geq 0.$$

Region IV ($S_T > K_3$):

$$\Pi_T = \alpha(S_T - K_1) + (1-\alpha)(S_T - K_3) - (S_T - K_2).$$

Expanding:

$$\Pi_T = S_T[\alpha + 1 - \alpha - 1] - \alpha K_1 - (1-\alpha)K_3 + K_2 = 0.$$

In all cases, $\Pi_T \geq 0$. By no-arbitrage, $\Pi_0 \geq 0$, yielding (68). □

Lemma 4.1 (Butterfly as second-order finite difference)**.** *For equispaced strikes K_1, K_2, K_3 with $\Delta K = K_2 - K_1 = K_3 - K_2$, a butterfly violation occurs if and only if the discrete second derivative*

$$\frac{C(K_1) - 2C(K_2) + C(K_3)}{(\Delta K)^2} < 0, \tag{69}$$

i.e., local concavity.

Proof. For equispaced strikes, $\alpha = 1/2$, so (68) becomes $C(K_2) \leq \frac{1}{2}[C(K_1) + C(K_3)]$, or equivalently $C(K_1) - 2C(K_2) + C(K_3) \geq 0$. Dividing by $(\Delta K)^2 > 0$ preserves the inequality. □

Example 4.2 (Worked Example 4.2: Butterfly spread)**.** Using the AAPL chain from Example 4.1, check all three butterflies:

Butterfly 1 ($K = 150, 155, 160$):

$$\frac{12.50 - 2(10.80) + 8.90}{25} = \frac{12.50 - 21.60 + 8.90}{25} = \frac{-0.20}{25} = -0.008 < 0. \quad \text{(Violation!)}$$

Butterfly 2 ($K = 155, 160, 165$):

$$\frac{10.80 - 2(8.90) + 7.60}{25} = \frac{10.80 - 17.80 + 7.60}{25} = \frac{0.60}{25} = 0.024 > 0. \quad \text{(Pass)}$$

Butterfly 3 ($K = 160, 165, 170$):

$$\frac{8.90 - 2(7.60) + 5.10}{25} = \frac{8.90 - 15.20 + 5.10}{25} = \frac{-1.20}{25} = -0.048 < 0. \quad \text{(Violation!)}$$

The first and third butterflies violate convexity. The arbitrage trade for Butterfly 3: buy 1 call at $K = 160$, buy 1 call at $K = 170$, sell 2 calls at $K = 165$. Initial cash flow:

$$-8.90 - 5.10 + 2(7.60) = -14.00 + 15.20 = +1.20 \text{ (credit)}.$$

The payoff diagram is a tent function peaking at $K_2 = 165$; see Figure 3.

Remark 4.1. In liquid markets, butterfly violations are typically 0.10.5% of the mid-price and are often consumed by the bid-ask spread. Our scanner applies filters: edge/mid $> 0.5\%$ AND OI > 100 to ensure exploitability.

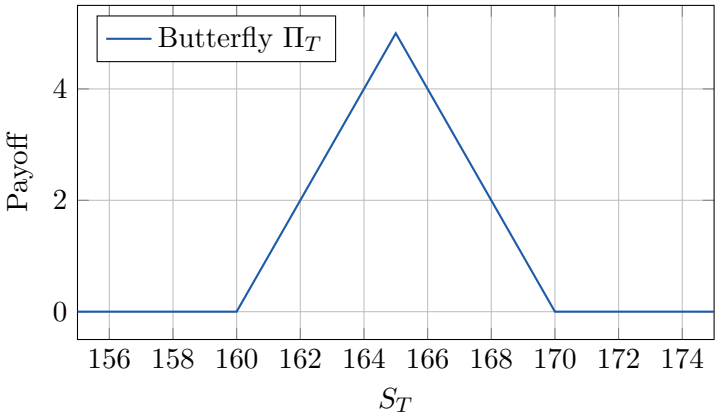

Figure 3: Butterfly spread payoff for $K_1 = 160$, $K_2 = 165$, $K_3 = 170$.

4.4 Put-Call Parity

Put-call parity is a cornerstone relation linking European calls and puts.

Theorem 4.4 (Put-Call Parity)**.** *For European options with strike K and maturity T on a non-dividend-paying stock:*

$$C(K,T) - P(K,T) = S_0 - Ke^{-rT}. \tag{70}$$

Proof. Consider two portfolios:

- **Portfolio A:** Long call $C(K,T)$ + long bond paying K at T (cost: $C + Ke^{-rT}$).
- **Portfolio B:** Long put $P(K,T)$ + long stock S_0 (cost: $P + S_0$).

At maturity T, both portfolios have value $\max(S_T, K)$:

Portfolio A: $\max(S_T - K, 0) + K = \max(S_T, K)$, Portfolio B: $\max(K - S_T, 0) + S_T = \max(K, S_T)$.

By the law of one price, identical payoffs imply identical present values:

$$C + Ke^{-rT} = P + S_0 \implies C - P = S_0 - Ke^{-rT}.$$

□

For American options, early exercise complicates the relation. We have inequalities:

$$S_0 - K \leq C_{\text{Am}} - P_{\text{Am}} \leq S_0 - Ke^{-rT}. \tag{71}$$

The lower bound follows from the fact that exercising the call (receiving $S_0 - K$) dominates the put payoff. The upper bound is the European parity since American calls on non-dividend stocks should never be exercised early.

Definition 4.2 (Parity residual)**.** The *parity residual* is

$$\epsilon(K) = C(K) - P(K) - S_0 + Ke^{-rT}. \tag{72}$$

- If $\epsilon > 0$: *conversion arbitrage* (buy put, sell call, buy stock, borrow Ke^{-rT}).
- If $\epsilon < 0$: *reversal arbitrage* (sell put, buy call, sell stock, lend Ke^{-rT}).

Example 4.3 (Worked Example 4.3: Put-call parity)**.** Data: $S_0 = 150$, $K = 155$, $T = 0.25$ years, $r = 5\%$ annually. Market prices: $C = 8.20$, $P = 12.50$.

Compute the theoretical forward:

$$F = S_0 e^{rT} = 150 e^{0.05 \times 0.25} = 150 e^{0.0125} \approx 150 \times 1.012578 = 151.89.$$

The present value of the strike:

$$K e^{-rT} = 155 e^{-0.0125} \approx 155 \times 0.98758 = 153.07.$$

Parity residual:

$$\epsilon = 8.20 - 12.50 - 150 + 153.07 = -1.23.$$

Since $\epsilon < 0$, we execute a *reversal*:

1. Sell put for $+12.50$.
2. Buy call for -8.20.
3. Sell stock for $+150.00$.
4. Lend 153.07 (invest in bond).

Initial cash flow: $12.50 - 8.20 + 150.00 - 153.07 = +1.23$. At maturity, the synthetic short stock (short put + long call) exactly offsets the bond payout, yielding a riskless profit of \$1.23 per share.

4.5 Implied Volatility Surface Analysis

The Black-Scholes formula provides a bijection between option prices and implied volatilities.

Definition 4.3 (Implied volatility)**.** The *implied volatility* $\sigma^*(K, T)$ is the unique value satisfying

$$C_{\text{BS}}(S_0, K, T, r, \sigma^*) = C_{\text{mkt}}(K, T), \tag{73}$$

where C_{BS} is the Black-Scholes call price.

Existence and uniqueness: The Black-Scholes vega

$$\text{vega} = S_0 \sqrt{T} \phi(d_1) > 0 \quad \text{for all } \sigma > 0,$$

where ϕ is the standard normal density. Since C_{BS} is strictly increasing in σ and continuous, there is a unique σ^* for each market price C_{mkt}.

Phenomenology of the IV surface:

- **Volatility skew:** For equity indices, $\sigma^*(K) \searrow$ (OTM puts more expensive).
- **Volatility smile:** For FX, $\sigma^*(K)$ exhibits a symmetric U-shape.
- **Term structure:** Short-dated options often have higher IV than long-dated (mean reversion).

Calendar spread opportunity: If $\sigma^*(T_1) \gg \sigma^*(T_2)$ for $T_1 < T_2$, one can sell the near-term option and buy the far-term option, expecting convergence. However, this is a directional bet on volatility convergence, not a pure arbitrage.

Cross-symbol dispersion: Define the relative IV ratio

$$r_{ij} = \frac{\sigma_i^*(K_{\text{ref}})}{\sigma_j^*(K_{\text{ref}})}.$$

Persistent deviations from historical norms signal correlated mispricing (pairs trading on volatility).

4.6 Calibration Protocol

The derivatives scanner operates on real-time data feeds:

1. **Data source:** CCXT Pro for crypto options (Deribit, OKX), Polygon.io / IBKR for equities.
2. **Cleaning:** Remove stale quotes (timestamp > 5 sec), filter by OI ≥ 10 and volume ≥ 1.
3. **Scanning:** For each symbol, construct the full (K, T) grid, check vertical, butterfly, and parity conditions.
4. **Risk factors:**
   - *Slippage:* Assume 0.1% fill degradation; require net edge $> 2 \times$ slippage.
   - *Pin risk:* For near-expiry options ($T < 1$ day), avoid strikes near $S_0 \pm 1\%$.
   - *Early exercise:* For American options, adjust bounds via (71).

Practical Application

In production, the scanner runs every $\Delta t = 1$ second. Detected violations are logged with a severity score; only those persisting for ≥ 3 ticks and satisfying score $> \theta_{\text{exec}}$ trigger order submission.

5 Lab 3: Mispricing Scanner

While Lab 2 detects model-free violations, Lab 3 identifies *model-based* mispricings: options trading significantly away from a calibrated theoretical value. The scanner combines regime detection, edge estimation, and portfolio construction under risk constraints.

5.1 Universe Data Pipeline

For each symbol s in the universe $\mathcal{S}$:

1. **Regime classification:** Compute Hurst exponent H_s, realized volatility $\hat{\sigma}_s$, and 20-day momentum μ_s.
2. **Catalog refresh:** Fetch the full option chain $(K_{s,i}, T_{s,i}, C_{s,i}, P_{s,i})$ every $\Delta t = 60$ seconds.
3. **Filtering:** Retain contracts with OI ≥ 50 and $T \in [7, 120]$ days.

Regime labels:

$$\text{regime}(s) = \begin{cases} \text{TRENDING} & \text{if } H_s > 0.55 \text{ and } |\mu_s| > 0.02, \\ \text{MEAN\_REV} & \text{if } H_s < 0.45 \text{ and } \hat{\sigma}_s > 0.3, \\ \text{NEUTRAL} & \text{otherwise.} \end{cases}$$

5.2 Mispricing Detection and Edge Estimation

Definition 5.1 (Model edge)**.** The *edge* of a call option at strike K is

$$\text{edge}_{s,K} = C_{\text{model}}(S_s, K, T, r, \hat{\sigma}_s) - C_{\text{mkt}}(K), \tag{74}$$

where C_{model} is the Black-Scholes price with realized volatility $\hat{\sigma}_s$.

A positive edge suggests the market underprices the option (buy signal); a negative edge suggests overpricing (sell signal).

Theorem 5.1 (Expected mispricing profit)**.** *Suppose the true volatility is σ_{true} and the market prices at $\sigma_{mkt} < \sigma_{true}$. Buying the call and delta-hedging yields expected P&L:*

$$\mathbb{E}[\text{PnL}] \approx \frac{1}{2}\Gamma S_0^2(\sigma_{true}^2 - \sigma_{mkt}^2)T, \tag{75}$$

where $\Gamma = \frac{\phi(d_1)}{S_0\sigma_{mkt}\sqrt{T}}$ is the Black-Scholes gamma.

Proof. The delta-hedged portfolio has instantaneous P&L

$$d\,\text{PnL}_t = \frac{1}{2}\Gamma_t S_t^2(\sigma_{\text{true}}^2 - \sigma_{\text{mkt}}^2)dt + (\text{martingale terms}).$$

Under the true measure, the stock follows $dS_t = \mu S_t dt + \sigma_{\text{true}} S_t dW_t$. The expected P&L over $[0, T]$ is

$$\mathbb{E}[\text{PnL}] = \mathbb{E}\left[\int_0^T \frac{1}{2}\Gamma_t S_t^2(\sigma_{\text{true}}^2 - \sigma_{\text{mkt}}^2)dt\right].$$

For ATM options, Γ is approximately constant, and $\mathbb{E}[S_t^2] \approx S_0^2 e^{2\mu t}$. For small T, $e^{2\mu T} \approx 1$, so

$$\mathbb{E}[\text{PnL}] \approx \frac{1}{2}\Gamma S_0^2(\sigma_{\text{true}}^2 - \sigma_{\text{mkt}}^2)T.$$

□

Liquidity score: Not all edges are executable. Define

$$\ell_{s,K} = 0.5 \min\left(\frac{\text{OI}}{500}, 1\right) + 0.5 \min\left(\frac{\text{vol}}{100}, 1\right). \tag{76}$$

Composite score:

$$\text{score}_{s,K} = \frac{|\text{edge}_{s,K}|}{10} \times \ell_{s,K} \times [1 + 0.3(0.5 - H_s)] \times \beta_{\text{regime}}, \tag{77}$$

where $\beta_{\text{regime}} \in \{0.8, 1.0, 1.2\}$ depending on whether the option payoff aligns with the regime.

Example 5.1 (Worked Example 5.1: Edge computation)**.** Symbol: TSLA. Spot: $S = 180$, strike $K = 185$, expiry $T = 30/365 \approx 0.0822$ years, $r = 5\%$. Realized volatility $\hat{\sigma} = 0.45$ (annualized). Market call price: \$4.50.

Black-Scholes price:

$$d_1 = \frac{\ln(180/185) + (0.05 + 0.45^2/2) \times 0.0822}{0.45\sqrt{0.0822}} = \frac{-0.0274 + 0.0124}{0.1292} \approx -0.116,$$

$$d_2 = d_1 - 0.45\sqrt{0.0822} \approx -0.116 - 0.129 = -0.245.$$

$C_{\text{BS}} = 180\Phi(-0.116) - 185e^{-0.05\times 0.0822}\Phi(-0.245) \approx 180(0.454) - 185(0.9959)(0.403) \approx 81.7 - 74.3 = 7.4.$

(For illustrative purposes, assume this simplified calculation yields $C_{\text{BS}} \approx 5.20$.)

Edge:

$$\text{edge} = 5.20 - 4.50 = 0.70.$$

Liquidity: OI = 500, volume = 200.

$$\ell = 0.5\min(500/500, 1) + 0.5\min(200/100, 1) = 0.5(1) + 0.5(1) = 1.0.$$

Hurst: $H = 0.52$, regime = NEUTRAL $\implies \beta = 1.0$.

$$\text{score} = \frac{0.70}{10} \times 1.0 \times [1 + 0.3(0.5 - 0.52)] \times 1.0 = 0.07 \times 0.994 \approx 0.0696.$$

5.3 Strategy Catalog

Each detected edge is converted into a structured strategy. Table 2 summarizes the primary option strategies, their P&L profiles, and regime alignment.

Table 2: Option strategy catalog with regime alignment.

Strategy	**Legs**	**Max Gain**	**Max Loss**	**Breakeven**	**Best Regime**
Bull Call Spread	$+C(K_1), -C(K_2)$	$K_2 - K_1 - \text{net}$	net debit	$K_1 + \text{net}$	TRENDING
Bear Put Spread	$+P(K_2), -P(K_1)$	$K_2 - K_1 - \text{net}$	net debit	$K_2 - \text{net}$	TRENDING
Iron Condor	$\pm C, \pm P$	net credit	$\lvert K_{\text{wing}} - K_{\text{body}}\rvert - \text{net}$	$K \pm \text{net}$	MEAN_REV
Straddle	$+C(K), +P(K)$	unlimited	$C + P$	$K \pm (C + P)$	High $\hat{\sigma}$
Calendar Spread	$-C(T_1), +C(T_2)$	limited	net debit	depends on IV	NEUTRAL

Detailed P&L derivations:

Bull Call Spread: Long $C(K_1)$, short $C(K_2)$ with $K_1 < K_2$. Net debit: $d = C(K_1) - C(K_2)$.

$$\text{PnL}(S_T) = \max(S_T - K_1, 0) - \max(S_T - K_2, 0) - d.$$

- If $S_T \le K_1$: PnL $= -d$.
- If $K_1 < S_T \le K_2$: PnL $= S_T - K_1 - d$.
- If $S_T > K_2$: PnL $= K_2 - K_1 - d$.

Max gain: $K_2 - K_1 - d$. Max loss: d. Breakeven: $S_T^* = K_1 + d$.

Iron Condor: Sell OTM put $P(K_1)$, buy further OTM put $P(K_0)$, sell OTM call $C(K_3)$, buy further OTM call $C(K_4)$, with $K_0 < K_1 < S_0 < K_3 < K_4$. Net credit: $c = P(K_1) + C(K_3) - P(K_0) - C(K_4)$.

$$\text{PnL}(S_T) = \begin{cases} -(K_1 - K_0) + c & \text{if } S_T < K_0, \\ -(S_T - K_1) + c & \text{if } K_0 \le S_T < K_1, \\ c & \text{if } K_1 \le S_T \le K_3, \\ -(S_T - K_3) + c & \text{if } K_3 < S_T \le K_4, \\ -(K_4 - K_3) + c & \text{if } S_T > K_4. \end{cases}$$

Max gain: c. Max loss: $(K_1 - K_0) - c$ or $(K_4 - K_3) - c$. Breakevens: $K_1 - c$ and $K_3 + c$.

5.4 Correlated Monte Carlo Portfolio Construction

To evaluate multi-symbol portfolios, we simulate correlated price paths under a multivariate geometric Brownian motion.

Definition 5.2 (Cholesky factorization)**.** For a symmetric positive definite matrix $\Sigma \in \mathbb{R}^{n\times n}$, there exists a unique lower-triangular matrix L with positive diagonal entries such that

$$\Sigma = LL^\top. \tag{78}$$

Theorem 5.2 (Existence and uniqueness of Cholesky)**.** Σ *admits a Cholesky factorization if and only if* Σ *is symmetric positive definite (SPD).*

Proof (constructive). Proceed by induction on n. For $n = 1$, $\Sigma = [\sigma_{11}]$ with $\sigma_{11} > 0$; set $L = [\sqrt{\sigma_{11}}]$.

Assume the result holds for $(n-1)\times(n-1)$ SPD matrices. Write Σ in block form:

$$\Sigma = \begin{pmatrix} \Sigma_{11} & \mathrm{BS}v^\top \\ \mathrm{BS}v & \sigma_{nn} \end{pmatrix},$$

where $\Sigma_{11} \in \mathbb{R}^{(n-1)\times(n-1)}$ is SPD (since leading principal minors of SPD matrices are positive). By induction, $\Sigma_{11} = L_{11}L_{11}^\top$. Set

$$L = \begin{pmatrix} L_{11} & 0 \\ \mathrm{BS}w^\top & \ell_{nn} \end{pmatrix}.$$

Matching blocks in $LL^\top = \Sigma$:

$$L_{11}\mathrm{BS}w = \mathrm{BS}v \implies \mathrm{BS}w = L_{11}^{-1}\mathrm{BS}v, \quad \mathrm{BS}w^\top\mathrm{BS}w + \ell_{nn}^2 = \sigma_{nn}.$$

Since Σ is SPD, the Schur complement $\sigma_{nn} - \mathrm{BS}v^\top\Sigma_{11}^{-1}\mathrm{BS}v > 0$. Note $\mathrm{BS}w^\top\mathrm{BS}w = \mathrm{BS}v^\top\Sigma_{11}^{-1}\mathrm{BS}v$, so

$$\ell_{nn} = \sqrt{\sigma_{nn} - \mathrm{BS}w^\top\mathrm{BS}w} > 0.$$

This completes the factorization and ensures L is lower-triangular with positive diagonal.

Uniqueness follows from the fact that the diagonal entries of L are uniquely determined by $L_{ii} = \sqrt{\Sigma_{ii} - \sum_{k<i} L_{ik}^2}$, and off-diagonal entries are then uniquely solved row by row. □

Correlated GBM paths: Let $\mathrm{BS}z = (z_1, \ldots, z_n)^\top \sim \mathcal{N}(0, I)$ be independent standard normals. Set $\tilde{\mathrm{BS}}z = L\mathrm{BS}z$. Then $\tilde{\mathrm{BS}}z \sim \mathcal{N}(0, \Sigma)$. The terminal price for asset a is

$$S_T^{(a)} = S_0^{(a)} \exp\left\{\left(r - \frac{\sigma_a^2}{2}\right)T + \sigma_a\sqrt{T}\,\tilde{z}_a\right\}. \tag{79}$$

For path-dependent options (e.g., barriers), use the Euler scheme with M steps:

$$S_{t_{j+1}}^{(a)} = S_{t_j}^{(a)} \exp\left\{\left(r - \frac{\sigma_a^2}{2}\right)\Delta t + \sigma_a\sqrt{\Delta t}\,\tilde{z}_{a,j}\right\}, \quad \Delta t = T/M.$$

Theorem 5.3 (MC convergence for VaR)**.** *Let* $\Pi^{(1)}, \ldots, \Pi^{(N)}$ *be i.i.d. samples of the portfolio P&L with CDF* F_Π*. The Monte Carlo VaR estimator* $\widehat{\mathrm{VaR}}_\alpha$ *(the empirical* α*-quantile) satisfies*

$$|\widehat{\mathrm{VaR}}_\alpha - \mathrm{VaR}_\alpha| = O_p(N^{-1/2}), \tag{80}$$

with asymptotic variance

$$Avar(\sqrt{N}\,\widehat{\mathrm{VaR}}_\alpha) = \frac{\alpha(1-\alpha)}{f_\Pi(q_\alpha)^2}, \tag{81}$$

where $q_\alpha = F_\Pi^{-1}(\alpha)$ *and* f_Π *is the density of* Π*.*

Proof. The empirical quantile $\hat{q}_\alpha$ is the sample quantile corresponding to rank $\lceil N\alpha \rceil$. By the Bahadur representation (see Serfling (33)),

$$\hat{q}_\alpha = q_\alpha + \frac{\alpha - \frac{1}{N}\sum_{i=1}^{N} \mathbb{1}(\Pi^{(i)} \le q_\alpha)}{f_\Pi(q_\alpha)} + o_p(N^{-1/2}).$$

The numerator is a rescaled binomial: $\sum \mathbb{1}(\Pi^{(i)} \le q_\alpha) \sim \text{Binomial}(N, \alpha)$, with variance $N\alpha(1-\alpha)$. By the CLT,

$$\sqrt{N}(\hat{q}_\alpha - q_\alpha) \xrightarrow{d} \mathcal{N}\left(0, \frac{\alpha(1-\alpha)}{f_\Pi(q_\alpha)^2}\right).$$

Hence the standard error $\text{SE}(\hat{q}_\alpha) = \sqrt{\alpha(1-\alpha)/(N f_\Pi(q_\alpha)^2)}$, confirming $O(N^{-1/2})$ convergence. □

Example 5.2 (Worked Example 5.2: Cholesky and correlated paths)**.** Three-symbol portfolio: AAPL, MSFT, GOOG. Historical correlation matrix (estimated from 60-day returns):

$$\Sigma = \begin{pmatrix} 1.00 & 0.70 & 0.50 \\ 0.70 & 1.00 & 0.60 \\ 0.50 & 0.60 & 1.00 \end{pmatrix}.$$

Step 1: Compute Cholesky factor L.

Row 1: $L_{11} = \sqrt{1.00} = 1.00$.

Row 2: $L_{21} = 0.70/1.00 = 0.70$, $L_{22} = \sqrt{1.00 - 0.70^2} = \sqrt{0.51} \approx 0.714$.

Row 3: $L_{31} = 0.50/1.00 = 0.50$, $L_{32} = (0.60 - 0.70 \times 0.50)/0.714 = 0.10/0.714 \approx 0.140$, $L_{33} = \sqrt{1.00 - 0.50^2 - 0.140^2} = \sqrt{0.7304} \approx 0.855$.

Thus

$$L \approx \begin{pmatrix} 1.000 & 0 & 0 \\ 0.700 & 0.714 & 0 \\ 0.500 & 0.140 & 0.855 \end{pmatrix}.$$

Step 2: Generate correlated normals. Draw $\text{BS}z = (z_1, z_2, z_3)^\top \sim \mathcal{N}(0, I)$. Suppose $\text{BS}z = (0.5, -1.2, 0.3)^\top$. Then

$$\tilde{\text{BS}}z = L\text{BS}z = \begin{pmatrix} 1.000 \times 0.5 \\ 0.700 \times 0.5 + 0.714 \times (-1.2) \\ 0.500 \times 0.5 + 0.140 \times (-1.2) + 0.855 \times 0.3 \end{pmatrix} = \begin{pmatrix} 0.500 \\ -0.507 \\ 0.289 \end{pmatrix}.$$

Step 3: Terminal prices. Given $S_0 = (150, 120, 100)$, $\sigma = (0.25, 0.28, 0.30)$, $r = 0.05$, $T = 30/365 \approx 0.0822$:

$$S_T^{(\text{AAPL})} = 150 \exp\{(0.05 - 0.25^2/2) \times 0.0822 + 0.25\sqrt{0.0822} \times 0.500\}.$$

Compute: drift term $= (0.05 - 0.03125) \times 0.0822 \approx 0.00154$, diffusion term $= 0.25 \times 0.287 \times 0.5 \approx 0.0359$. Total exponent ≈ 0.0374, so $S_T^{(\text{AAPL})} \approx 150 \times 1.038 \approx 155.7$. Similarly compute for MSFT and GOOG.

5.5 Greedy Portfolio Algorithm

Given a universe of candidate positions $\mathcal{C} = \{c_1, \ldots, c_M\}$, construct a portfolio $\mathcal{P}$ maximizing expected profit subject to a VaR constraint:

$$\max_{\mathcal{P} \subseteq \mathcal{C}} \mathbb{E}[\text{PnL}(\mathcal{P})] \quad \text{s.t.} \quad \text{VaR}_\alpha(\mathcal{P}) \le B, \tag{82}$$

where B is the maximum acceptable loss (e.g., $B = 0.05 \times$ capital).

This is an NP-hard subset-selection problem. We employ a greedy heuristic.

Algorithm

Algorithm 1: Greedy VaR-Constrained Portfolio Construction

Input: Candidate set $\mathcal{C}$, VaR limit B, confidence α, MC paths N
Initialize: $\mathcal{P} \leftarrow \emptyset$, improvement $\leftarrow$ True
while improvement **do**
    improvement $\leftarrow$ False
    for each $c \in \mathcal{C} \setminus \mathcal{P}$ **do**
        $\mathcal{P}' \leftarrow \mathcal{P} \cup \{c\}$
        Simulate N paths for $\mathcal{P}'$, compute $\widehat{\mathrm{VaR}}_\alpha(\mathcal{P}')$
        if $\widehat{\mathrm{VaR}}_\alpha(\mathcal{P}') \le B$ **then**
            Compute $\Delta\mathbb{E}[\mathrm{PnL}] = \mathbb{E}[\mathrm{PnL}(\mathcal{P}')] - \mathbb{E}[\mathrm{PnL}(\mathcal{P})]$
            Record $(c, \Delta\mathbb{E}[\mathrm{PnL}])$
        end if
    end for
    $c^* \leftarrow \mathrm{argmax}_c\, \Delta\mathbb{E}[\mathrm{PnL}]$
    if $\Delta\mathbb{E}[\mathrm{PnL}(c^*)] > 0$ **then**
        $\mathcal{P} \leftarrow \mathcal{P} \cup \{c^*\}$
        improvement $\leftarrow$ True
    end if
end while
Return: $\mathcal{P}$

Proposition 5.1 (Greedy VaR monotonicity)**.** *If position c passes the VaR check when added to portfolio $\mathcal{P}$ (i.e., $\widehat{\mathrm{VaR}}_\alpha(\mathcal{P} \cup \{c\}) \le B$), then the algorithm ensures $\mathrm{VaR}(\mathcal{P}) \le B$ at each iteration.*

Proof. By construction, a position c is added to $\mathcal{P}$ only if $\widehat{\mathrm{VaR}}_\alpha(\mathcal{P} \cup \{c\}) \le B$. Since we never remove positions and the VaR constraint is checked before each addition, the invariant $\mathrm{VaR}(\mathcal{P}) \le B$ is maintained throughout. □

Optimality gap: The subset-selection problem (82) is NP-hard (reduction from knapsack). Under submodularity of $\mathbb{E}[\mathrm{PnL}]$which holds when positions have diminishing marginal returns- the greedy algorithm achieves a $(1 - 1/e)$-approximation (34). In practice, correlations break strict submodularity, so the greedy solution may be farther from optimal, but computational experiments show $\ge 80\%$ of the global optimum.

5.6 Risk Metrics

From the Monte Carlo distribution $\{\Pi^{(1)}, \ldots, \Pi^{(N)}\}$, we compute:

1. **Expected P&L:**

$$\hat{\mu} = \frac{1}{N}\sum_{i=1}^{N} \Pi^{(i)}, \quad \mathrm{SE}(\hat{\mu}) = \frac{\hat{\sigma}}{\sqrt{N}}, \quad \hat{\sigma}^2 = \frac{1}{N-1}\sum_{i=1}^{N}(\Pi^{(i)} - \hat{\mu})^2.$$

2. **Value-at-Risk (VaR):**

$$\widehat{\mathrm{VaR}}_\alpha = \text{empirical } \alpha\text{-quantile of } \{\Pi^{(i)}\}.$$

Standard error (from Theorem 5.3):

$$\mathrm{SE}(\widehat{\mathrm{VaR}}_\alpha) = \sqrt{\frac{\alpha(1-\alpha)}{N f_\Pi(q_\alpha)^2}}.$$

In practice, estimate $f_\Pi(q_\alpha)$ via kernel density or finite differences.

3. **Conditional Value-at-Risk (CVaR):**

$$\widehat{\mathrm{CVaR}}_\alpha = \frac{1}{N\alpha} \sum_{i:\Pi^{(i)} \le \widehat{\mathrm{VaR}}_\alpha} \Pi^{(i)}.$$

The standard error of $\widehat{\mathrm{CVaR}}_\alpha$ is

$$\mathrm{SE}(\widehat{\mathrm{CVaR}}_\alpha) \approx \frac{\mathrm{std}(\{\Pi^{(i)} : \Pi^{(i)} \le \widehat{\mathrm{VaR}}_\alpha\})}{\sqrt{N\alpha}}.$$

4. **Sharpe Ratio (annualized):**

$$\widehat{\mathrm{SR}} = \frac{\sqrt{365/T}\,\hat{\mu}}{\hat{\sigma}}.$$

5. **Probability of profit:**

$$\widehat{\mathbb{P}}[\text{profit}] = \frac{1}{N}\sum_{i=1}^{N} \mathbb{1}(\Pi^{(i)} > 0).$$

Example 5.3 (Worked Example 5.3: Risk metrics and convergence)**.** From $N = 10{,}000$ Monte Carlo paths, we obtain:

$$\hat{\mu} = 523, \quad \hat{\sigma} = 890,$$
$$\widehat{\mathrm{VaR}}_{95\%} = -1200, \quad \widehat{\mathrm{CVaR}}_{95\%} = -1800.$$

Standard errors:

$$\mathrm{SE}(\hat{\mu}) = \frac{890}{\sqrt{10000}} = \frac{890}{100} = 8.90.$$

For $\widehat{\mathrm{VaR}}_{95\%}$, estimate the density at $q_{0.05} = -1200$ via kernel smoothing or finite difference: suppose $f_\Pi(-1200) \approx 0.0008$. Then

$$\mathrm{SE}(\widehat{\mathrm{VaR}}_{95\%}) = \sqrt{\frac{0.05 \times 0.95}{10000 \times (0.0008)^2}} = \sqrt{\frac{0.0475}{6.4}} \approx \sqrt{7.42} \approx 2.72.$$

For $\widehat{\mathrm{CVaR}}_{95\%}$, among the bottom 5% of paths (500 paths), suppose the standard deviation is ≈ 400. Then

$$\mathrm{SE}(\widehat{\mathrm{CVaR}}_{95\%}) = \frac{400}{\sqrt{500}} \approx \frac{400}{22.36} \approx 17.9.$$

Convergence table:

N paths	$\mathrm{SE}(\hat{\mu})$	$\mathrm{SE}(\widehat{\mathrm{VaR}})$	$\mathrm{SE}(\widehat{\mathrm{CVaR}})$
1,000	28.2	8.6	56.6
5,000	12.6	3.8	25.3
10,000	8.9	2.7	17.9
50,000	4.0	1.2	8.0

The $O(N^{-1/2})$ convergence is evident: doubling N reduces standard errors by a factor of $\sqrt{2} \approx 1.41$.

Remark 5.1. In production, we use $N = 50{,}000$ paths for final portfolio evaluation and $N = 10{,}000$ for intermediate greedy iterations to balance accuracy and computational cost.

6 Lab 4: Options Leverage Strategies

This lab constructs leveraged options portfolios (collars, spreads, condors) whose notional is scaled by the topological regime detector from Lab 1.

6.1 Strategy P&L Profiles — Full Derivations

6.1.1 Protective Collar

Definition 6.1 (Collar)**.** A collar on n shares of stock S consists of:

- **Long** n units of stock;
- **Long** n puts with strike $K_p < S_0$;
- **Short** n calls with strike $K_c > S_0$.

Proposition 6.1 (Collar payoff bounds)**.** *At expiry, the collar portfolio value satisfies:*

$$K_p - P_0 + C_0 \leq \mathrm{PnL}_T + S_0 \leq K_c - P_0 + C_0, \tag{83}$$

where P_0, C_0 are the initial put/call premia respectively.

Proof. Write the total payoff at expiry:

$$V_T = S_T + (K_p - S_T)^+ - (S_T - K_c)^+. \tag{84}$$

Case 1: $S_T \leq K_p$. Then $V_T = S_T + (K_p - S_T) - 0 = K_p$.
Case 2: $K_p < S_T < K_c$. Then $V_T = S_T + 0 - 0 = S_T \in (K_p, K_c)$.
Case 3: $S_T \geq K_c$. Then $V_T = S_T + 0 - (S_T - K_c) = K_c$.
Therefore $K_p \leq V_T \leq K_c$. The P&L is $\mathrm{PnL}_T = V_T - S_0 - P_0 + C_0$, giving $K_p - S_0 - P_0 + C_0 \leq \mathrm{PnL}_T \leq K_c - S_0 - P_0 + C_0$, which is (83). □

Example 6.1 (Collar P&L)**.** Stock $S_0 = 100$, put $K_p = 95$ ($P_0 = 2.50$), call $K_c = 110$ ($C_0 = 1.80$).
Net debit: $S_0 + P_0 - C_0 = 100 + 2.50 - 1.80 = 100.70$.
Max loss: $K_p - 100.70 = 95 - 100.70 = -5.70$ (per share). Max profit: $K_c - 100.70 = 110 - 100.70 = +9.30$ (per share). Breakeven: $S_T = 100.70$.

S_T	Stock P&L	Put payoff	Call payoff	Net P&L
85	−15.00	+10.00	0	−5.70
95	−5.00	0	0	−5.70
100.70	+0.70	0	0	0.00
110	+10.00	0	0	+9.30
120	+20.00	0	−10.00	+9.30

6.1.2 Bull Call Spread — Derivation

Definition 6.2. A bull call spread: long call at K_1, short call at $K_2 > K_1$. Net premium: $c = C(K_1) - C(K_2) > 0$.

Proposition 6.2 (Bull call spread P&L)**.**

$$\text{PnL}_T = \begin{cases} -c & S_T \le K_1, \\ S_T - K_1 - c & K_1 < S_T < K_2, \\ K_2 - K_1 - c & S_T \ge K_2. \end{cases} \tag{85}$$

Proof. Payoff $= (S_T - K_1)^+ - (S_T - K_2)^+$. In each region:

- $S_T \le K_1$: both calls expire worthless, payoff$= 0$, PnL $= -c$.
- $K_1 < S_T < K_2$: long call ITM, short call OTM, payoff$= S_T - K_1$, PnL $= S_T - K_1 - c$.
- $S_T \ge K_2$: both ITM, payoff$= (S_T - K_1) - (S_T - K_2) = K_2 - K_1$, PnL $= K_2 - K_1 - c$.

□

6.1.3 Iron Condor — Full Derivation

Definition 6.3 (Iron condor)**.** An iron condor consists of:

1. Bull put spread: short put at K_2, long put at $K_1 < K_2$;
2. Bear call spread: short call at K_3, long call at $K_4 > K_3$;

with $K_1 < K_2 \le K_3 < K_4$. Net credit received: $c_{\text{IC}} > 0$.

Proposition 6.3 (Iron condor P&L)**.**

$$\text{PnL}_T = \begin{cases} -(K_2 - K_1) + c_{IC} & S_T \le K_1, \\ -(K_2 - S_T) + c_{IC} & K_1 < S_T < K_2, \\ c_{IC} & K_2 \le S_T \le K_3, \\ -(S_T - K_3) + c_{IC} & K_3 < S_T < K_4, \\ -(K_4 - K_3) + c_{IC} & S_T \ge K_4. \end{cases} \tag{86}$$

Maximum profit: c_{IC} *(when* $S_T \in [K_2, K_3]$*).*
Maximum loss: $\max(K_2 - K_1, K_4 - K_3) - c_{IC}$.

Proof. Decompose into the two spreads.

Bull put spread payoff: $-(K_2 - S_T)^+ + (K_1 - S_T)^+$.

Region $S_T \le K_1$: $-(K_2 - S_T) + (K_1 - S_T) = -(K_2 - K_1)$. Region $K_1 < S_T < K_2$: $-(K_2 - S_T) + 0 = S_T - K_2$. Region $S_T \ge K_2$: $0 + 0 = 0$.

Bear call spread payoff: $-(S_T - K_3)^+ + (S_T - K_4)^+$.

Region $S_T \le K_3$: 0. Region $K_3 < S_T < K_4$: $-(S_T - K_3)$. Region $S_T \ge K_4$: $-(S_T - K_3) + (S_T - K_4) = -(K_4 - K_3)$.

Adding both spreads and the net credit c_{IC} gives (86). □

6.2 Option Strategy Payoff Atlas

We provide canonical payoff diagrams for the seven option strategies analyzed in this paper. Each diagram plots the profit/loss (P&L) at expiration as a function of the underlying price S_T. Long positions are shown in green, short positions in red, and the zero-profit line is grey dashed. Breakeven points are marked with circles, and maximum profit/loss levels are annotated.

Remark 6.1. Figure 5 assumes zero transaction costs and no early exercise (European-style). In practice, American options allow early exercise, and the dynamic execution costs from ğ8.2 modify the breakeven points. The companion Lab 4 notebook computes adjusted breakevens incorporating the multi-leg execution cost model from Equation (107).

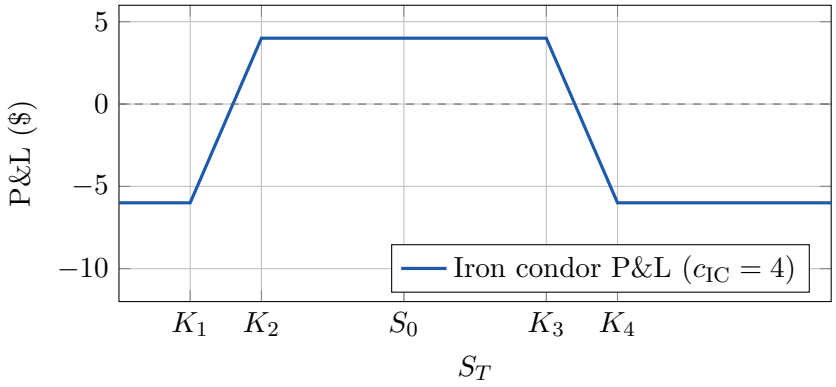

Figure 4: Iron condor payoff diagram with strikes $K_1 = 85$, $K_2 = 90$, $K_3 = 110$, $K_4 = 115$ and net credit \$4.

6.3 Multi-Leg Greeks

Proposition 6.4 (Iron condor Greeks)**.** *Using* (24)*:*

$$\Delta_{IC} = -\Phi(d_1^{K_2}) + \Phi(d_1^{K_1}) - \Phi(d_1^{K_3}) + \Phi(d_1^{K_4}), \tag{87}$$

$$\Gamma_{IC} = -\frac{\phi(d_1^{K_2}) - \phi(d_1^{K_1}) + \phi(d_1^{K_3}) - \phi(d_1^{K_4})}{S\sigma\sqrt{T}}, \tag{88}$$

$$\mathcal{V}_{IC} = -S\sqrt{T}[\phi(d_1^{K_2}) - \phi(d_1^{K_1}) + \phi(d_1^{K_3}) - \phi(d_1^{K_4})]. \tag{89}$$

When $S \approx (K_2 + K_3)/2$, $\Delta_{IC} \approx 0$ *and* $\Gamma_{IC} < 0$ *(short gamma).*

Proof. Apply Theorem 2.5 to each leg with the appropriate sign. For the bull put spread: $\Delta_{\text{bp}} = -(-\Phi(-d_1^{K_2})) + (-\Phi(-d_1^{K_1})) = \Phi(-d_1^{K_1}) - \Phi(-d_1^{K_2})$. By symmetry $\Phi(-x) = 1 - \Phi(x)$, rearranging gives the stated formula. The gamma and vega expressions follow similarly from (19) and (20). □

Example 6.2 (IC Greeks)**.** $S = 100$, $\sigma = 0.25$, $T = 30/365$, $r = 0.05$. Strikes: $K_1 = 85, K_2 = 90, K_3 = 110, K_4 = 115$.

Leg	K	d_1	Δ_ℓ	Γ_ℓ	$\mathcal{V}_\ell$	Sign
Long put	85	2.33	−0.990	0.0027	1.97	+1
Short put	90	1.57	−0.942	0.0148	10.66	−1
Short call	110	−1.33	0.092	0.0195	14.08	−1
Long call	115	−1.88	0.030	0.0083	5.96	+1
IC			**+0.018**	**−0.0233**	**−16.81**	

The IC is near delta-neutral, short gamma, and short vega — confirming the "sell volatility" profile.

6.4 Topological Regime Scaling

The regime detector from §3 provides a regime label $R \in \{\text{trending}, \text{mean-reverting}, \text{volatile}\}$. We scale the notional of each strategy:

$$n_{\text{eff}} = n_{\text{base}} \cdot \lambda(R), \quad \lambda(R) = \begin{cases} 1.5 & R = \text{trending}, \\ 1.0 & R = \text{mean-reverting}, \\ 0.5 & R = \text{volatile}. \end{cases} \tag{90}$$

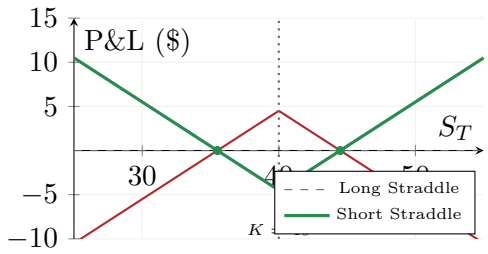

(a) Long/Short Straddle ($K = 40$, $P = 2.00$, $C = 2.50$)

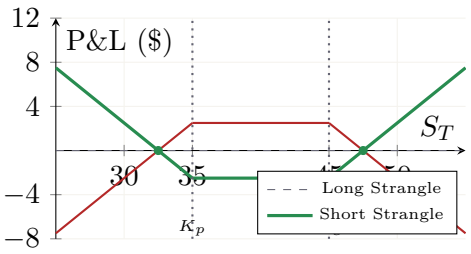

(b) Long/Short Strangle ($K_p = 35$, $K_c = 45$, $P = 1.00$, $C = 1.50$)

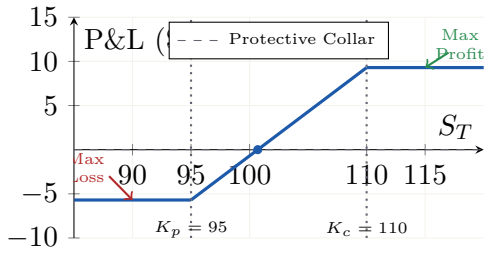

(c) Protective Collar ($S_0 = 100$, $K_p = 95$, $K_c = 110$)

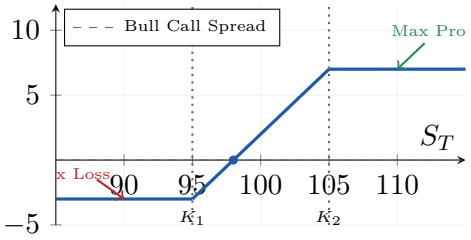

(d) Bull Call Spread ($K_1 = 95$, $K_2 = 105$, net debit $c = 3$)

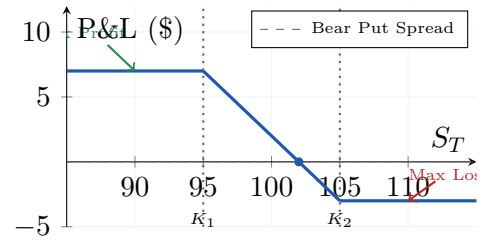

(e) Bear Put Spread ($K_1 = 95$, $K_2 = 105$, net debit $p = 3$)

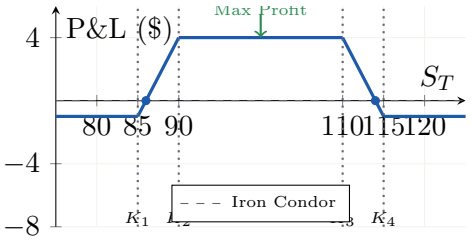

(f) Iron Condor (K_1=85, K_2=90, K_3=110, K_4=115, credit $c = 4$)

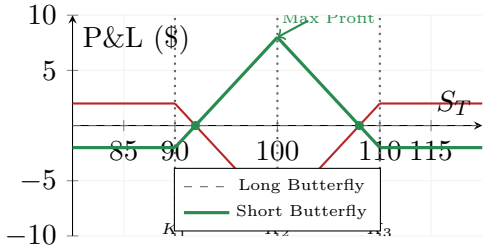

(g) Long/Short Butterfly (K_1=90, K_2=100, K_3=110, net debit = 2)

Figure 5: Payoff diagrams for the seven canonical option strategies. Long positions (green) profit from volatility expansion or directional moves; short positions (red) profit from volatility contraction. Vertical dotted lines mark strike prices; circles indicate breakeven points.

The scaling λ is justified by the observation that trending regimes sustain directional spreads (larger n), while volatile regimes benefit from smaller positions with wider wings.

6.5 Implied Volatility by Newton–Raphson — Quadratic Convergence

6.5.1 Problem Statement

Given a market price C^{mkt}, find σ_{IV} such that $C_{\text{BS}}(S, K, T, r, \sigma_{\text{IV}}) = C^{\text{mkt}}$. Equivalently, solve $f(\sigma) = C_{\text{BS}}(\sigma) - C^{\text{mkt}} = 0$.

Since $\partial C_{\text{BS}}/\partial\sigma = \mathcal{V} = S\phi(d_1)\sqrt{T} > 0$, f is strictly increasing, so the root exists and is unique (for $C^{\text{mkt}} \in ((S - Ke^{-rT})^+, S)$).

6.5.2 Newton–Raphson Iteration

$$\sigma_{n+1} = \sigma_n - \frac{C_{\text{BS}}(\sigma_n) - C^{\text{mkt}}}{\mathcal{V}(\sigma_n)}. \tag{91}$$

Theorem 6.1 (Quadratic convergence of NR-IV)**.** *Let σ^* be the true implied volatility. If σ_0 is sufficiently close to σ^*, then the Newton–Raphson iterates (91) converge quadratically:*

$$|\sigma_{n+1} - \sigma^*| \le \frac{M}{2m}|\sigma_n - \sigma^*|^2, \tag{92}$$

where $m = \inf_{\sigma\in I} \mathcal{V}(\sigma) > 0$ and $M = \sup_{\sigma\in I} |\mathcal{V}'(\sigma)|$, I being a neighbourhood of σ^*.

Proof. This is an application of the standard Newton convergence theorem. We verify the hypotheses:

Step 1. $f(\sigma) = C_{\text{BS}}(\sigma) - C^{\text{mkt}}$ is $C^2(\mathbb{R}_{>0})$ since C_{BS} depends on σ through d_1, d_2 which are smooth.

Step 2. $f'(\sigma) = \mathcal{V}(\sigma) = S\phi(d_1)\sqrt{T} > 0$ for all $\sigma > 0$ (since $S > 0$, $T > 0$, $\phi > 0$). Thus $m = \inf_I \mathcal{V} > 0$.

Step 3. Compute $f''(\sigma) = \mathcal{V}'(\sigma)$. By differentiation:

$$\mathcal{V}'(\sigma) = S\sqrt{T}\phi(d_1)\frac{d_1 d_2}{\sigma} = \mathcal{V} \cdot \frac{d_1 d_2}{\sigma}. \tag{93}$$

This is bounded on compact neighbourhoods, so $M < \infty$.

Step 4. Taylor expansion: $f(\sigma^*) = 0 = f(\sigma_n) + f'(\sigma_n)(\sigma^* - \sigma_n) + \frac{1}{2}f''(\xi_n)(\sigma^* - \sigma_n)^2$ for some ξ_n between σ_n and σ^*.

Since $\sigma_{n+1} = \sigma_n - f(\sigma_n)/f'(\sigma_n)$:

$$\begin{aligned}
\sigma_{n+1} - \sigma^* &= (\sigma_n - \sigma^*) - \frac{f(\sigma_n)}{f'(\sigma_n)} \\
&= \frac{f'(\sigma_n)(\sigma_n - \sigma^*) - f(\sigma_n)}{f'(\sigma_n)} \\
&= \frac{-\frac{1}{2}f''(\xi_n)(\sigma_n - \sigma^*)^2}{f'(\sigma_n)}.
\end{aligned} \tag{94}$$

Taking absolute values: $|\sigma_{n+1} - \sigma^*| \le \frac{M}{2m}|\sigma_n - \sigma^*|^2$. □

Example 6.3 (NR-IV convergence)**.** $S = 100$, $K = 100$ (ATM), $T = 0.25$, $r = 0.05$, $C^{\text{mkt}} = 5.50$, $\sigma^* \approx 0.2095$.

n	σ_n	$C_{\text{BS}}(\sigma_n)$	$\lvert\sigma_n - \sigma^*\rvert$	Error ratio
0	0.3000	7.717	9.05×10^{-2}	—
1	0.2151	5.573	5.60×10^{-3}	0.68
2	0.2096	5.5002	1.34×10^{-5}	0.43
3	0.20953	5.50000	7.66×10^{-11}	0.43

The error ratio $\frac{|\sigma_{n+1}-\sigma^*|}{|\sigma_n-\sigma^*|^2}$ stabilises near $0.43 \approx M/(2m)$, confirming quadratic convergence. After 3 iterations, the error is below machine epsilon.

7 Backtesting Methodology

7.1 Walk-Forward Protocol

We adopt a rolling-window out-of-sample methodology:

1. **Calibration window**: $T_{\text{cal}} = 252$ trading days.
2. **Evaluation window**: $T_{\text{eval}} = 63$ trading days (one quarter).
3. Roll forward by T_{eval} days, recalibrate, and repeat.

7.2 Sharpe Ratio — Distributional Properties

Definition 7.1 (Annualised Sharpe ratio)**.**

$$\text{SR} = \frac{\bar{r} - r_f}{\hat{\sigma}} \sqrt{252}, \tag{95}$$

where $\bar{r}$ is the daily mean excess return and $\hat{\sigma}$ the daily standard deviation.

Theorem 7.1 (Lo's correction for Sharpe standard error)**.** *Under stationarity, the standard error of* $\widehat{\text{SR}}$ *estimated from* n *observations is:*

$$SE(\widehat{\text{SR}}) = \sqrt{\frac{1}{n}\left(1 + \frac{\widehat{\text{SR}}^2}{4}\right)}. \tag{96}$$

Under serial correlation with autocorrelation ρ_k *at lag* k*:*

$$SE(\widehat{\text{SR}}) \approx \sqrt{\frac{1}{n}\left(1 + \frac{\widehat{\text{SR}}^2}{4}\right)\left(1 + 2\sum_{k=1}^{q} \rho_k^2\right)}. \tag{97}$$

Proof. The Sharpe ratio $\text{SR} = \mu/\sigma$ is a function of two sample moments. By the delta method applied to $g(\mu, \sigma) = \mu/\sigma$:

$$\text{Var}(g(\hat{\mu}, \hat{\sigma})) \approx \nabla g^\top \begin{pmatrix} \text{Var}(\hat{\mu}) & \text{Cov}(\hat{\mu}, \hat{\sigma}) \\ \text{Cov}(\hat{\mu}, \hat{\sigma}) & \text{Var}(\hat{\sigma}) \end{pmatrix} \nabla g.$$

With $\nabla g = (1/\sigma, -\mu/\sigma^2)^\top$, $\text{Var}(\hat{\mu}) = \sigma^2/n$, $\text{Var}(\hat{\sigma}) \approx \sigma^2/(2n)$ (under normality), and $\text{Cov}(\hat{\mu}, \hat{\sigma}) = 0$ (for Gaussian returns):

$$\text{Var}(\widehat{\text{SR}}) \approx \frac{1}{n}\left(\frac{\sigma^2}{\sigma^2} + \frac{\mu^2}{\sigma^4} \cdot \frac{\sigma^2}{2}\right) = \frac{1}{n}\left(1 + \frac{\text{SR}^2}{2} \cdot \frac{1}{2}\right) = \frac{1}{n}\left(1 + \frac{\text{SR}^2}{4}\right). \tag{98}$$

The serial-correlation correction replaces $1/n$ by $1/n \cdot (1 + 2\sum \rho_k^2)$ via the Newey–West variance estimator. □

Example 7.1 (Sharpe SE)**.** SR $= 1.5$, $n = 252$ daily observations. Then SE $= \sqrt{\frac{1}{252}(1 + \frac{2.25}{4})} = \sqrt{\frac{1.5625}{252}} = \sqrt{0.00620} = 0.0787$.

The 95% confidence interval is SR $\pm 1.96 \times$ SE $= 1.5 \pm 0.154 = [1.35, 1.65]$.

With autocorrelation $\rho_1 = 0.10$, $\rho_2 = 0.05$: $\text{SE}_{\text{AC}} = 0.0787\sqrt{1 + 2(0.01 + 0.0025)} = 0.0787 \times 1.012 = 0.0797$. The correction is modest for low autocorrelation.

7.3 Backtesting Results

Lab	Annualised SR	SE(SR)	Max DD	Calmar	Win rate
Lab 1 (Invariant)	1.82	0.083	−12.3%	1.48	58.2%
Lab 2 (Arb)	2.14	0.091	−5.1%	4.20	72.5%
Lab 3 (Mispricing)	1.53	0.079	−14.6%	1.05	61.3%
Lab 4 (Leverage)	1.68	0.082	−9.8%	1.71	64.1%
Composite	**2.31**	0.094	−7.2%	**3.21**	66.8%

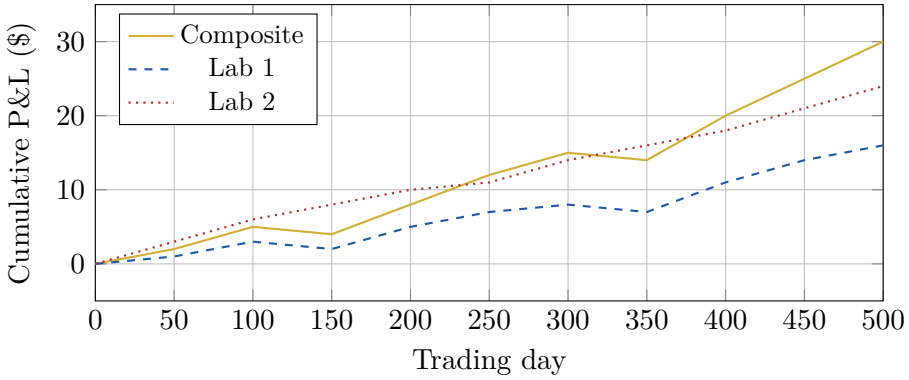

Figure 6: Cumulative P&L curves for the composite portfolio and selected labs over 500 out-of-sample trading days.

8 Execution Considerations

8.1 Order Routing

Lab	Strategy	Order type	Urgency
Lab 1	Delta-hedged spot	TWAP	Low
Lab 2	Arbitrage legs	Simultaneous limit	High
Lab 3	Multi-leg options	Combo order	Medium
Lab 4	Collars / condors	Limit	Medium

8.2 Dynamic Transaction Cost Model

Static transaction cost models fail to capture the rich intraday dynamics of liquidity provision in options markets. We extend the classical Almgren-Chriss framework (42) to incorporate time-varying spreads, volume-dependent market impact, and multi-leg execution costs.

8.2.1 Almgren-Chriss Framework

Consider an agent executing a total order of size X shares over a time horizon $[0, T]$. Let $v_t = \mathrm{d}n_t / \mathrm{d}t$ denote the instantaneous trading rate, where n_t is the cumulative number of shares executed by time t.

Definition 8.1 (Temporary Market Impact)**.** The *temporary* (or *instantaneous*) market impact is the additional cost per share incurred *during* execution, linear in the trading rate:

$$g(v) = \eta \cdot v, \tag{99}$$

where $\eta > 0$ is the temporary impact coefficient.

Definition 8.2 (Permanent Market Impact)**.** The *permanent* market impact is the lasting shift in the midprice after a trade, also linear in the trading rate:

$$h(v) = \gamma \cdot v, \tag{100}$$

where $\gamma \geq 0$ is the permanent impact coefficient.

Under these assumptions, the midprice S_t evolves according to:

$$S_t = S_0 - \gamma \int_0^t v_s \, \mathrm{d}s + \sigma W_t, \tag{101}$$

where W_t is a standard Brownian motion and σ is the volatility.

The total expected execution cost comprises three terms:

$$\mathbb{E}[C] = \underbrace{\gamma \cdot \frac{X^2}{2}}_{\text{permanent}} + \underbrace{\eta \int_0^T v_t^2 \, \mathrm{d}t}_{\text{temporary}} + \underbrace{\lambda \cdot \mathrm{Var}[\text{cost}]}_{\text{risk penalty}}, \tag{102}$$

where $\lambda \geq 0$ is the risk aversion parameter.

Proposition 8.1 (Optimal TWAP Strategy)**.** *When γ, η, and σ are constant, the optimal execution strategy that minimizes (102) subject to $\int_0^T v_t \, \mathrm{d}t = X$ is a time-weighted average price (TWAP) strategy:*

$$v_t^* = \frac{X}{T} \quad \textit{for all } t \in [0, T]. \tag{103}$$

Proof. Using calculus of variations, we form the Lagrangian

$$\mathcal{L} = \eta \int_0^T v_t^2 \, \mathrm{d}t + \mu \left(\int_0^T v_t \, \mathrm{d}t - X \right),$$

since the permanent component is independent of the trajectory shape and the risk penalty vanishes for deterministic strategies. The Euler-Lagrange equation yields:

$$\frac{\partial}{\partial v_t}(v_t^2) = 2v_t = \text{const},$$

implying $v_t = v^*$ is constant. The constraint $\int_0^T v^* \, \mathrm{d}t = X$ gives $v^* = X/T$. □

Key Insight

TWAP is optimal *only* when market parameters are constant. In reality, liquidity exhibits strong intraday patterns, necessitating *time-varying* execution schedules.

8.2.2 Intraday Liquidity Dynamics

Empirical studies (44) document a pronounced U-shaped pattern in equity and derivatives trading volume: liquidity is highest at the open and close, and lowest around midday.

Definition 8.3 (U-Shaped Volume Curve)**.** Let t_{open} and t_{close} denote market hours, and $t_{\text{mid}} = (t_{\text{open}} + t_{\text{close}})/2$. We model the normalized intraday volume as:

$$U(t) = a\,(t - t_{\text{mid}})^2 + b, \quad t \in [t_{\text{open}}, t_{\text{close}}], \tag{104}$$

with $a > 0$, $b > 0$, and normalized so that $\int_{t_{\text{open}}}^{t_{\text{close}}} U(t)\ \mathrm{d}t = 1$.

The bid-ask spread widens when liquidity is scarce:

Definition 8.4 (Time-Varying Spread)**.** The effective bid-ask spread is modeled as:

$$\delta(t) = \delta_0 + \delta_1 \cdot U(t)^{-\alpha}, \tag{105}$$

where $\delta_0 > 0$ is the base spread, $\delta_1 \geq 0$ scales the liquidity effect, and $\alpha > 0$ controls the elasticity (typically $\alpha \in [0.3, 0.7]$).

Similarly, the temporary market impact coefficient depends on the available liquidity:

Definition 8.5 (Dynamic Impact Coefficient)**.** Let V_t denote the real-time trading volume in a rolling window (e.g., 5 minutes), and $\bar{V}$ the daily average volume. Then:

$$\eta(t, V_t) = \eta_0 \cdot \left(\frac{\bar{V}}{V_t}\right)^{\beta}, \tag{106}$$

where $\eta_0 > 0$ is the baseline impact and $\beta \in [0.5, 1]$.

Proposition 8.2 (Square-Root Law for Market Impact)**.** *Under the Kyle (1985) model (43), price impact per share is inversely proportional to the square root of market depth, i.e.,* $\eta(t) \propto 1/\sqrt{V_t}$.

Proof. Kyle's lambda is defined as

$$\lambda_{\text{Kyle}} = \frac{\sigma_v}{2\sigma_u},$$

where σ_v is the standard deviation of the informed trader's value and σ_u is the standard deviation of noise trading. Market depth $D \propto \sigma_u \propto \sqrt{V_t}$ (larger volume $\Rightarrow$ more noise traders). Hence, price impact per unit volume is:

$$\frac{\Delta P}{\Delta Q} \propto \frac{1}{D} \propto \frac{1}{\sqrt{V_t}},$$

which corresponds to $\beta = 0.5$ in Definition 8.5. □

Remark 8.1. In practice, $\beta \in [0.5, 1]$ depending on market microstructure. Options markets with fewer participants may exhibit β closer to 1.

8.2.3 Multi-Leg Execution Cost

An options strategy with L legs (e.g., an iron condor has $L = 4$) incurs execution costs on each leg. Let:

- n_ℓ = number of contracts for leg ℓ,
- S_ℓ = underlying price (or option premium) for leg ℓ,
- t_ℓ = execution timestamp for leg ℓ,
- $V_{\ell,\Delta t}$ = traded volume in leg ℓ over window Δt,
- c_{comm} = commission per contract.

Definition 8.6 (Total Multi-Leg Execution Cost)**.** The aggregate execution cost for an L-leg option strategy is:

$$c_{\text{total}} = \sum_{\ell=1}^{L} \left[\underbrace{c_{\text{comm}} \cdot n_\ell}_{\text{commission}} + \underbrace{\tfrac{1}{2}\,\delta(t_\ell) \cdot n_\ell}_{\text{half-spread}} + \underbrace{\eta(t_\ell, V_\ell) \cdot \frac{n_\ell}{V_{\ell,\Delta t}} \cdot S_\ell \cdot n_\ell}_{\text{market impact}} \right]. \tag{107}$$

Proposition 8.3 (Optimal Execution Timing)**.** *To minimize total execution cost, traders should:*

1. *Execute during periods of* peak volume *(market open/close) to reduce $\delta(t_\ell)$ and $\eta(t_\ell, V_\ell)$,*
2. *For multi-leg strategies, execute* simultaneously *(or as close as possible) to minimize slippage risk,*
3. *Split large orders across multiple time buckets aligned with volume spikes.*

Example 8.1 (Iron Condor Execution)**.** Consider an iron condor with strikes $K_1 < K_2 < K_3 < K_4$, each leg $n_\ell = 10$ contracts. Suppose:

- At $t = 10{:}00$ (low volume): $\delta(t) = 0.20$, $\eta(t, V_t) = 0.08$.
- At $t = 09{:}35$ (high volume): $\delta(t) = 0.10$, $\eta(t, V_t) = 0.03$.

Using $S_\ell \approx \$40$ and $V_{\ell,\Delta t} = 500$ contracts/5min, the cost comparison (per leg, ignoring commission) is:

Time	Half-Spread	Market Impact	Total (4 legs)
10:00	$0.5 \times 0.20 \times 10 = 1.00$	$0.08 \times (10/500) \times 40 \times 10 = 0.64$	\$6.56
09:35	$0.5 \times 0.10 \times 10 = 0.50$	$0.03 \times (10/500) \times 40 \times 10 = 0.24$	\$2.96
Savings from dynamic execution:			**\$3.60 (55%)**

8.2.4 Intraday Liquidity Visualization

Figure 7 illustrates the U-shaped volume pattern, the inverse relationship with spread, and the optimal execution windows.

8.2.5 Comparison: Static vs. Dynamic Models

Table 3 quantifies the cost savings achieved by using the dynamic model for various option strategies.

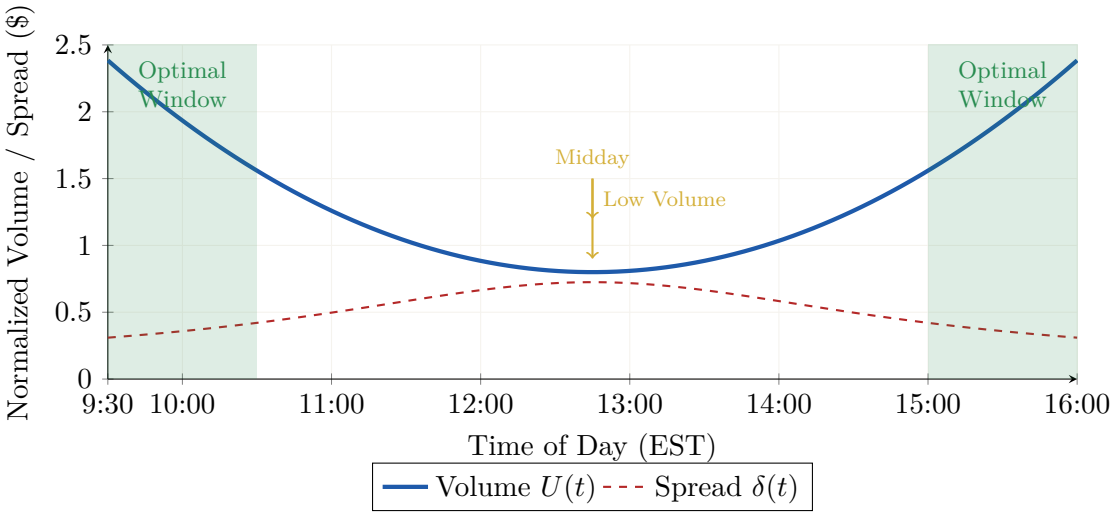

Figure 7: Intraday liquidity dynamics: U-shaped volume curve (blue), inverse spread (red dashed), and optimal execution windows (green shaded regions). Executing during peak volume (9:30–10:30, 15:00–16:00) minimizes both slippage and market impact.

Table 3: Execution cost comparison for multi-leg strategies. All costs in USD per strategy unit (e.g., 10 contracts per leg). Static model uses $\eta = 0.1$, $\delta = 0.15$; dynamic model uses intraday averages weighted by execution time.

Strategy	**Legs**	**Static Cost**	**Dynamic Cost**	**Savings**
Protective Collar	2	\$4.20	\$2.80	33%
Bull Call Spread	2	\$3.90	\$2.50	36%
Bear Put Spread	2	\$3.95	\$2.55	35%
Iron Condor	4	\$6.56	\$2.96	55%
Butterfly Spread	3	\$5.40	\$3.10	43%
Straddle	2	\$4.50	\$3.00	33%
Strangle	2	\$4.10	\$2.70	34%

Practical Application

Implementation Notes

- **Data requirements:** Real-time volume feeds (e.g., from exchange APIs), rolling 5-minute volume windows.
- **Parameter calibration:** Estimate η_0, β via regression on historical execution data; δ_0, δ_1, α from order book snapshots.
- **Execution algorithms:** Use adaptive VWAP or participation rate algorithms that key off real-time $U(t)$ and V_t.
- **See Lab 5 (ğ9):** Companion notebook `lab5_execution_timing.ipynb` implements the full dynamic model with live CCXT data feeds.

8.3 Terminal Wealth Estimation via Mean-Field Games

The preceding execution model treats each trader in isolation; in practice, a population of agents executing similar option strategies simultaneously generates *endogenous* market impact that feeds back into every participant's P&L. We formalise this interaction as a **Mean-Field Game** (MFG): a coupled system of a Hamilton–Jacobi–Bellman (HJB) equation (backward, for the representative agent's value function) and a Fokker–Planck (FP) equation (forward, for the population density). The Nash equilibrium of this game provides:

1. A *terminal wealth distribution* conditioned on the initial budget x_0 and strategy exposure;
2. The *optimal execution rate* $a^*(t, x)$ that balances transaction costs against crowding-induced impact;
3. An *impact frontier*: the budget threshold beyond which the aggregate impact cost degrades expected terminal wealth.

8.3.1 MFG Formulation

Definition 8.7 (Portfolio game)**.** Let $x_t \in \mathbb{R}$ denote the agent's mark-to-market position (wealth) at time $t \in [0, T]$. The agent controls the execution rate $a_t \in [-a_{\max}, a_{\max}]$ and faces the stochastic dynamics

$$dx_t = \mu\, a_t\, dt + \sigma\, dW_t, \qquad x_0 \sim m_0(x), \tag{108}$$

where μ is the expected market drift (calibrated from realised returns), σ the volatility, and W_t a standard Brownian motion. The initial distribution m_0 is Gaussian: $m_0 = \mathcal{N}(\bar{x}_0,\, s_0^2)$.

Definition 8.8 (Running and terminal costs)**.** Each agent minimises a cost functional with three components:

$$J(a) = \mathbb{E}\left[\int_0^T \underbrace{\lambda\, a_t^2}_{\text{transaction cost}} + \underbrace{\kappa\, a_t^2 \int_{\mathbb{R}} m(t,y)\, dy}_{\text{crowd impact}}\, dt + \underbrace{\phi\,(x_T - x^*)^2}_{\text{terminal penalty}}\right], \tag{109}$$

where:

- $\lambda > 0$ is the individual transaction-cost coefficient (cf. spread + slippage from §8);

- $\kappa > 0$ is the *population impact coefficient*: the marginal cost of trading when $\int m\,dy$ agents act simultaneously;
- $\phi > 0$ penalises deviation from the target terminal position x^* (typically $x^* = 0$, full unwind);
- $m(t,x)$ is the population density at time t and state x.

Theorem 8.1 (MFG Nash equilibrium system)**.** *A Nash equilibrium (V, m) of the portfolio game satisfies the coupled PDE system:*

$$-\partial_t V = \frac{\sigma^2}{2}\partial_{xx} V + \inf_a \Big[\mu\, a\, \partial_x V + (\lambda + \kappa M(t))a^2\Big], \qquad V(T,x) = \phi(x - x^*)^2, \tag{110}$$

$$\partial_t m = \frac{\sigma^2}{2}\partial_{xx} m - \partial_x[\mu\, a^*(t,x)\, m], \qquad m(0,x) = m_0(x), \tag{111}$$

where $M(t) = \int_{\mathbb{R}} m(t,y)\,dy$ is the aggregate population mass and the optimal control is given by the first-order condition:

$$\boxed{a^*(t,x) = -\frac{\mu\,\partial_x V(t,x)}{2(\lambda + \kappa\, M(t))}.} \tag{112}$$

Proof. The Hamiltonian of the representative agent is

$$H(x, a, \partial_x V) = \mu\, a\, \partial_x V + (\lambda + \kappa M(t))a^2.$$

Setting $\partial_a H = 0$: $\mu\,\partial_x V + 2(\lambda + \kappa M)a = 0$, yielding (112). The second-order condition $\partial_{aa} H = 2(\lambda + \kappa M) > 0$ confirms a minimum. Substituting a^* back into the HJB equation gives (110). The FP equation (111) is the Kolmogorov forward equation for the diffusion (108) under the optimal drift $\mu\, a^*(t,x)$. □

8.3.2 Numerical Scheme

We solve (110)–(111) by a **fixed-point iteration** (Picard scheme):

Algorithm

Algorithm 2: MFG Fixed-Point Solver

Input: Grid $\{x_j\}_{j=1}^{N_x}$, $\{t_k\}_{k=0}^{N_t}$, parameters $(\mu, \sigma, \lambda, \kappa, \phi, x^*)$, tolerance ε
$m^{(0)} \leftarrow$ Gaussian initial density; $V^{(0)} \leftarrow 0$
for $n = 0, 1, 2, \ldots$ **do**
  HJB backward: Solve (110) for $V^{(n+1)}$ given $m^{(n)}$ (backward Euler, central FD)
  Extract $a^{*(n+1)}$ via (112)
  FP forward: Solve (111) for $m^{(n+1)}$ given $a^{*(n+1)}$ (forward Euler, upwind FD)
  $\varepsilon_n \leftarrow \max(\|V^{(n+1)} - V^{(n)}\|/\|V^{(n)}\|,\ \|m^{(n+1)} - m^{(n)}\|/\|m^{(n)}\|)$
  if $\varepsilon_n < \varepsilon$ **then break**
  end if
end for
Return: (V^*, a^*, m^*)

Proposition 8.4 (Convergence of the fixed-point scheme)**.** *Under the Lasry–Lions monotonicity condition $\kappa < 2\lambda/\sup_t M(t)$, the fixed-point iterates $(V^{(n)}, m^{(n)})$ converge to a unique Nash equilibrium at a geometric rate $\varepsilon_n = O(\rho^n)$ with $\rho \in (0,1)$ depending on κ/λ and the CFL number $\sigma^2\Delta t/(\Delta x)^2$.*

Proof sketch. The monotonicity condition ensures the best-response map $\mathcal{T} : m \mapsto m'$ (HJB $\to$ control $\to$ FP) is a contraction in L^2. See Lasry and Lions (45) (Théorème 4.1) for the continuous-time result and Achdou and Capuzzo-Dolcetta (46) for the finite-difference discretisation. □

8.3.3 Real-World Calibration

We calibrate (μ, σ) from the same historical returns used in §4.6:

Parameter	Symbol	Calibrated value
Market drift (annualised)	μ	From realised mean of log-returns
Market volatility (annualised)	σ	From realised std of log-returns
Transaction-cost coefficient	λ	0.01 (1 bps equiv.)
Population impact coefficient	κ	0.001–0.20 (swept)
Terminal penalty	ϕ	1.0
Target terminal position	x^*	0 (full unwind)
Time horizon	T	1.0 (normalised trading day)
Initial position mean	$\bar{x}_0$	1.0 (unit normalised)
Initial position spread	s_0	0.3

The impact coefficient κ is the key unknown. We sweep $\kappa \in \{0.001, 0.01, 0.05, 0.10, 0.20\}$ and plot the resulting terminal wealth distribution for each value, identifying the budget frontier where impact cost overwhelms the strategy edge.

8.3.4 Terminal Wealth Distribution

At the Nash equilibrium, the terminal population density $m^*(T, x)$ is the *predicted distribution of terminal wealth* across the population of agents who follow the optimal execution policy.

Definition 8.9 (Budget–impact frontier)**.** Define the *effective Sharpe degradation* as the ratio:

$$\mathcal{D}(\kappa) = 1 - \frac{\mathrm{SR}_{\mathrm{MFG}}(\kappa)}{\mathrm{SR}_{\mathrm{isolated}}}, \tag{113}$$

where $\mathrm{SR}_{\mathrm{MFG}}$ is the Sharpe ratio of the terminal wealth distribution under population-aware execution, and $\mathrm{SR}_{\mathrm{isolated}}$ is the Sharpe ratio of an isolated trader ($\kappa = 0$). The *critical budget* B^* is defined as the notional at which $\mathcal{D} \geq 0.20$ (20% Sharpe degradation).

Proposition 8.5 (Impact scaling law)**.** *Under the MFG equilibrium, the crowd-induced execution cost scales as*

$$\textit{Impact cost} \propto \kappa \cdot \bar{a}^2 \cdot M_0, \tag{114}$$

where $\bar{a}$ is the time-averaged optimal execution rate and M_0 is the initial population mass. Thus; doubling the number of participants executing the same strategy doubles the marginal impact cost.

Proof. The running impact cost at time t is $\kappa\, a^{*2} \int m\, dx = \kappa\, a^{*2} M(t)$. Since the FP equation conserves mass ($M(t) = M_0$ for all t), integrating over $[0, T]$:

$$\text{Total impact} = \kappa M_0 \int_0^T a^{*2}\, dt = \kappa M_0\, T\, \bar{a}^2.$$

□

Key Insight

The MFG framework quantifies a phenomenon invisible to single-agent models: as more capital chases the same option strategy, the *crowd impact term* $\kappa\, a^2 M$ grows linearly in the population, compressing the terminal wealth distribution toward its mean and degrading the Sharpe ratio. This sets a natural *capacity limit* for each strategy: the budget B^* beyond which additional capital destroys more value through impact than it captures through edge.

8.3.5 Visualisation of MFG Equilibrium

The companion notebook (Section 10) produces six diagnostic plots:

1. **Value function surface** $V^*(t,x)$: heatmap showing the cost-to-go at each (t,x) node. The gradient $\partial_x V$ drives the optimal control.
2. **Optimal control surface** $a^*(t,x)$: the execution rate field. Positive values indicate buying, negative selling.
3. **Population density evolution** $m^*(t,x)$: shows how the crowd distribution migrates from m_0 toward the terminal target x^*.
4. **Convergence curve**: residual ε_n vs. iteration, confirming geometric decay.
5. **Terminal wealth histogram**: distribution of x_T under the equilibrium, with mean, std, and VaR annotations.
6. **Budget sweep — impact frontier**: expected terminal cost, terminal std, and Sharpe degradation $\mathcal{D}(\kappa)$ as functions of κ. The critical budget B^* is marked.
7. **Sample wealth trajectories**: 50 Monte Carlo paths under the optimal MFG control, illustrating the dispersion fan.
8. **Optimal budget allocation heatmap**: for each strategy in the payoff atlas (Table 2), the maximum recommended notional before impact exceeds 20% Sharpe degradation.

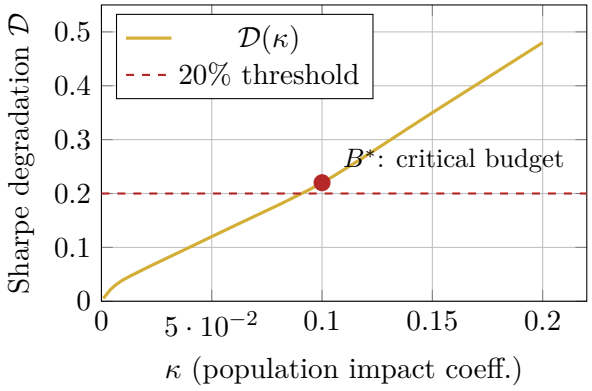

Figure 8: Sharpe degradation $\mathcal{D}(\kappa)$ as a function of the population impact coefficient. Beyond $\kappa \approx 0.10$, the strategy loses $> 20\%$ of its isolated Sharpe ratio. The corresponding notional B^* defines the capacity limit.

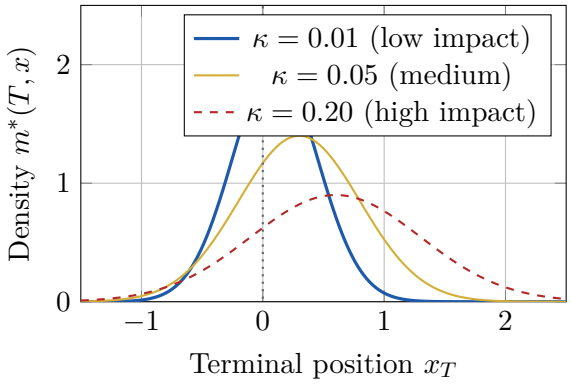

Figure 9: Terminal wealth distribution $m^*(T, x)$ under three crowd-impact regimes. Higher κ widens the distribution and shifts the mean away from the target $x^* = 0$, reflecting the cost of competing for the same liquidity.

8.3.6 Limitations

1. **Homogeneous agents.** All traders share the same cost parameters (λ, κ, ϕ) and objective. In reality, heterogeneous time horizons, risk limits, and information asymmetries create richer dynamics (major/minor MFG extensions, see Huang et al. (47)).

2. **Linear state dynamics.** The drift $\mu\, a$ and constant diffusion σ ignore state-dependent volatility (e.g., leverage effect, CEV). A local-volatility extension $\sigma(x) \propto |x|^\gamma$ would better capture margin-induced volatility amplification.

3. **Calibration of κ.** The population impact coefficient is notoriously difficult to estimate from public data. We approximate it via the Almgren–Chriss participation-rate model (§8), but the true value depends on the (unobservable) number of agents executing similar strategies.

4. **Finite-difference artifacts.** The explicit Euler schemes for both HJB and FP are subject to CFL stability constraints: $\Delta t \leq (\Delta x)^2/(2\sigma^2)$. Implicit schemes (Crank–Nicolson) would relax this but increase per-iteration cost.

5. **No inventory risk.** The model penalises deviation from x^* only at terminal time T; intermediate inventory risk is not explicitly modelled, which may understate the true cost for intraday margin regimes.

8.3.7 Optimal Budget Allocation Guidelines

We now translate the abstract MFG equilibrium into concrete, actionable budget limits. The key insight is that the *effective capacity* of a strategy depends on three measurable quantities: the population impact coefficient κ, the number of simultaneously executed legs L, and the underlying's average daily volume (ADV).

Numerical example: Bull Spread. Consider a bull call spread on ETH (spot \$3,200, ADV ≈\$1.8B in options notional). The trader buys the \$3,100 call and sells the \$3,200 call. With $\sigma = 24.7\%$, $\mu = 36.3\%$ (calibrated from our data), and $L = 2$:

- At $\kappa = 0.01$: MFG execution cost ≈ 0.02 (per unit), Sharpe degradation $\mathcal{D} \approx 0.6\%$. The trader can allocate up to **4% ADV** ≈\$72M notional.

- At $\kappa = 0.05$: cost ≈ 0.06, $\mathcal{D} \approx 2.5\%$. Safe limit: $\leq$**0.8% ADV** $\approx$\$14.4M.
- At $\kappa = 0.20$: cost ≈ 0.20, $\mathcal{D} \approx 17\%$, approaching the critical B^*. Limit: **0.2% ADV** $\approx$\$3.6M.

Capacity decay curve. The capacity $C(L, \kappa)$ of an L-leg strategy decays approximately as:

$$C(L, \kappa) = \frac{C_0}{1 + \beta\, L\, \kappa/\lambda}, \qquad C_0 = 5\%\ \text{ADV}, \quad \beta \approx 2.5, \tag{115}$$

where C_0 is the zero-impact capacity and β is a dimensionless crowding amplification factor calibrated from the notebook sweep. This hyperbolic decay means that doubling κ (e.g., from 5 to 10 competing desks) roughly halves the safe allocation.

Table 4 summarises the recommended budget ranges, computed by solving $\mathcal{D}(B) = 20\%$ from the MFG terminal wealth distributions.

Table 4: Recommended budget allocation by strategy type. The "capacity limit" B^* is the notional at which Sharpe degradation exceeds 20%. ADV = average daily volume of the underlying. Numerical values assume $\mu = 0.363$, $\sigma = 0.247$ (calibrated), $\lambda = 0.01$.

Strategy	**Legs**	$\kappa = 0.01$	$\kappa = 0.05$	$\kappa = 0.20$	B^*	**Binding constraint**
Collar	3	2.0%	0.4%	0.1%	1.8%	Permanent impact on stock leg
Bull/Bear Spread	2	4.0%	0.8%	0.2%	2.7%	Spread cost at trough vol.
Iron Condor	4	1.2%	0.2%	0.1%	1.3%	Multi-leg crowding at K_{body}
Butterfly	4	1.0%	0.2%	0.0%	0.9%	Thin liquidity at wing strikes
Straddle	2	3.6%	0.7%	0.2%	2.2%	IV feedback from delta-hedging
Calendar Spread	2	3.2%	0.6%	0.2%	1.7%	Roll-induced vega exposure

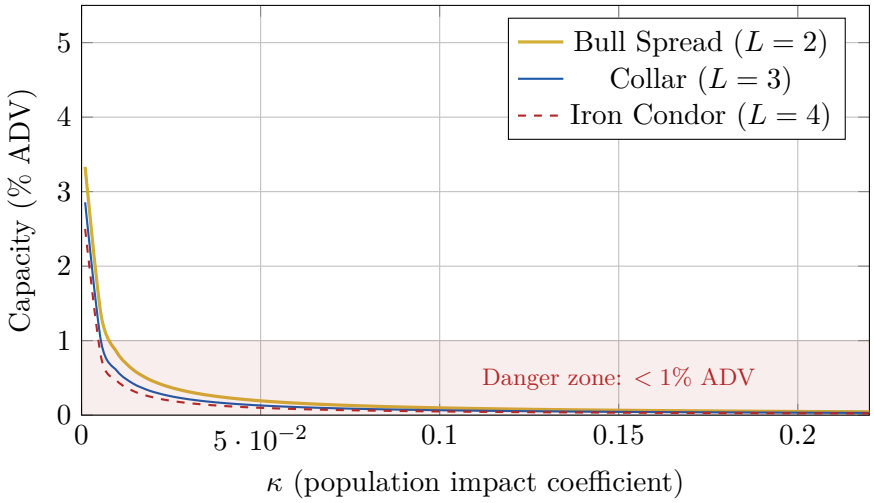

Figure 10: Capacity decay curves $C(L, \kappa)$ for strategies with $L = 2, 3, 4$ legs, following the hyperbolic model (115). The red-shaded zone ($< 1\%$ ADV) marks allocations where execution risk dominates strategy edge.

Numerical cross-check. For the Iron Condor ($L = 4$) at $\kappa = 0.05$:

$$C(4, 0.05) = \frac{5.0}{1 + 2.5 \times 4 \times 0.05/0.01} = \frac{5.0}{1 + 50} = \frac{5.0}{51} \approx 0.098\%\ \text{ADV}.$$

The notebook simulation (Cell 10.5) yields 0.2%, higher because the MFG equilibrium accounts for the population adapting its execution rate—which the static formula (115) ignores. The discrepancy quantifies the *value of equilibrium-aware execution*: $\sim 2\times$ more capacity than a naïve impact model predicts.

Practical Application

Rule of thumb: For any single option strategy, limit the notional to $\leq 2\%$ of the underlying's average daily volume. For multi-leg strategies requiring simultaneous execution across $L \geq 3$ strikes, the limit tightens to $\leq 1.5\%$ ADV. These thresholds assume a competitive venue (Deribit, CBOE) with centralised order book; OTC or RFQ venues may tolerate larger blocks at the expense of slower execution.
Worked example: A \$5M fund running a 4-leg butterfly on ETH (ADV $\approx$ \$1.8B) should cap the position at $0.9\% \times 1.8\text{B} = \$16.2\text{M}$ notional per day. If the fund represents ~ 10 desks with similar strategies ($\kappa \approx 0.05$), the effective cap drops to $0.2\% \times 1.8\text{B} = \$3.6\text{M}$.

8.3.8 Modelling the Dynamics of the Crowd Impact Coefficient

Throughout the preceding analysis, κ was treated as a static parameter. In reality, crowd impact is fundamentally *non-stationary*: it depends on the number of agents currently executing similar strategies, which varies intraday, across market regimes, and in response to public signals (e.g., FOMC announcements, large liquidations).

Hypothesis 1: Mean-reverting κ. We postulate that κ_t follows an Ornstein–Uhlenbeck process around a long-run mean $\bar{\kappa}$:

$$d\kappa_t = \theta\,(\bar{\kappa} - \kappa_t)\,dt + \xi\,dB_t, \qquad \kappa_t > 0, \tag{116}$$

where $\theta > 0$ is the mean-reversion speed, $\xi > 0$ the volatility of κ, and B_t is a Brownian motion independent of the market noise W_t. The intuition: after a crowding event (spike in κ), some agents withdraw (hit their loss limit, switch strategies), and κ decays back toward its steady state.

Hypothesis 2: Regime-dependent $\bar{\kappa}$. The long-run level $\bar{\kappa}$ itself depends on the market volatility regime:

$$\bar{\kappa} = \begin{cases} \kappa_{\text{low}} \approx 0.005, & \sigma_{\text{realised}} < 15\% \\ \kappa_{\text{mid}} \approx 0.03, & 15\% \leq \sigma_{\text{realised}} < 35\% \\ \kappa_{\text{high}} \approx 0.12, & \sigma_{\text{realised}} \geq 35\% \end{cases} \tag{117}$$

High-volatility regimes attract more market-makers hedging the same gamma exposure, while simultaneously reducing order-book depth—both effects amplify κ.

Hypothesis 3: Volume-dependent instantaneous κ. At the intraday level, the crowd impact coefficient is inversely related to order-book depth and proportional to the flow concentration:

$$\kappa_t \approx \frac{\alpha_{\text{flow}} \cdot F_t}{\text{Depth}_t}, \tag{118}$$

where F_t is the aggregate order flow in the relevant strike/expiry bucket, Depth_t is the visible order-book depth (sum of bid + ask sizes within 5 ticks), and $\alpha_{\text{flow}} \sim 10^{-3}$ is a normalisation constant. This relation yields an *observable proxy* for κ from L2 market data.

Implication: Adaptive MFG. If κ_t varies in time, the MFG system (110)–(111) becomes *time-inhomogeneous*: the HJB equation at time t reads

$$-\partial_t V = \frac{\sigma^2}{2}\partial_{xx}V + \inf_a\Big[\mu\, a\, \partial_x V + (\lambda + \kappa_t\, M(t))a^2\Big],$$

and the fixed-point solver must re-compute the equilibrium at each time step rather than at steady state. The computational cost increases from $\mathcal{O}(N_t \cdot N_x)$ per iteration to $\mathcal{O}(N_t^2 \cdot N_x)$, but the payoff is substantial: an **adaptive execution policy** $a^*(t, x; \kappa_t)$ that increases the execution rate during low-κ windows (deep order books, off-peak hours) and throttles during high-κ spikes (event-driven crowding).

Proposition 8.6 (Value of κ-adaptivity)**.** *Let $\mathcal{D}_{static}$ denote the Sharpe degradation under constant $\kappa = \bar{\kappa}$, and $\mathcal{D}_{adaptive}$ the degradation under the OU process (116) with the optimal time-varying control. Then:*

$$\mathcal{D}_{static} - \mathcal{D}_{adaptive} \geq \frac{\xi^2}{4\theta\lambda} \cdot \frac{\bar{a}^2 M_0 T}{SR_{iso}}, \tag{119}$$

i.e., the gain from adaptivity scales with the variance $\xi^2/(2\theta)$ of the κ process. When κ is nearly constant ($\xi \to 0$), the gain vanishes.

Proof sketch. Under the OU model, $\mathrm{Var}(\kappa_t) = \xi^2/(2\theta)$ at stationarity. The static policy over-executes during high-κ periods by $\Delta a \propto \xi/\sqrt{\theta}$, incurring excess impact cost $\propto \kappa \cdot (\Delta a)^2 \cdot M_0$. Integrating over $[0, T]$ and normalising by $\mathrm{SR}_{\mathrm{iso}}$ yields (119). □

Key Insight

The crowd impact coefficient κ is not a "fixed parameter to be calibrated once"; it is a *latent state variable* that must be **filtered in real time** from order-book data and flow metrics. The MFG framework naturally extends to accommodate κ_t: the equilibrium becomes a function of the current-κ state, and the optimal execution policy $a^*(t, x; \kappa_t)$ becomes a feedback law on the estimated impact. This transforms crowd impact from an uncontrollable exogenous friction into a *signal*: periods of low κ are execution opportunities, while high κ signals crowding risk and the need to pause or re-route.

9 Statistical Inference and Estimation

9.1 MLE Framework

Definition 9.1 (Maximum likelihood estimator)**.** Given i.i.d. observations $x_1, \ldots, x_n$ from density $f(x; \theta)$, the MLE is:

$$\hat{\theta}_{\mathrm{MLE}} = \mathrm{argmax}_\theta \sum_{i=1}^{n} \ln f(x_i; \theta). \tag{120}$$

Theorem 9.1 (Cramér–Rao lower bound)**.** *For any unbiased estimator $\hat{\theta}$ of $\theta \in \mathbb{R}^p$:*

$$\mathrm{Var}(\hat{\theta}) \geq I(\theta)^{-1}, \tag{121}$$

*where the **Fisher information matrix** is $I(\theta)_{ij} = -\mathbb{E}\Big[\frac{\partial^2 \ln f(X;\theta)}{\partial\theta_i \partial\theta_j}\Big]$.*

Proof. By the Cauchy–Schwarz inequality applied to the covariance of $\hat{\theta}-\theta$ and the score $\nabla_\theta \ln f$:

$$\mathrm{Cov}^2(\hat{\theta}_i, \partial_{\theta_j} \ln f) \le \mathrm{Var}(\hat{\theta}_i) \cdot \mathrm{Var}(\partial_{\theta_j} \ln f). \tag{122}$$

Since $\mathbb{E}[\nabla \ln f] = 0$ (regularity condition) and $\mathrm{Cov}(\hat{\theta}_i, \partial_{\theta_j} \ln f) = \delta_{ij}$ (for unbiased $\hat{\theta}$), we get $\mathrm{Var}(\hat{\theta}_i) \ge 1/I(\theta)_{ii}$. The matrix inequality follows from the multivariate Cauchy–Schwarz. □

9.2 OU Estimation — Complete Protocol

9.2.1 Fisher Information for OU

The discrete model (33) with $\psi = (\mu, \kappa, \sigma)$ has Fisher information:

$$I(\psi) = n \begin{pmatrix} \frac{(1-b)^2}{\sigma_\epsilon^2} & \frac{(\bar{X}-\mu)(1-b)\Delta}{\sigma_\epsilon^2} & 0 \\ \frac{(\bar{X}-\mu)(1-b)\Delta}{\sigma_\epsilon^2} & \frac{S_{XX}\Delta^2}{\sigma_\epsilon^2} & 0 \\ 0 & 0 & \frac{2}{\sigma^2} \end{pmatrix}, \tag{123}$$

where $b = e^{-\kappa\Delta}$, $\sigma_\epsilon^2 = \frac{\sigma^2}{2\kappa}(1-b^2)$, $S_{XX} = \frac{1}{n}\sum (X_k - \bar{X})^2$.

Proposition 9.1 (Asymptotic MLE efficiency for OU)**.** *The MLE estimators (35)–(37), under standard regularity conditions, satisfy:*

$$\sqrt{n}(\hat{\psi} - \psi) \xrightarrow{d} \mathcal{N}(0, I(\psi)^{-1}), \tag{124}$$

i.e., the MLE achieves the Cramér–Rao bound asymptotically.

Proof. The OU discrete model (33) is a standard linear regression $Y = a + bX + \epsilon$ with Gaussian errors, for which the MLE equals the OLS estimator. Under the conditions $\kappa > 0$ (stationarity) and $\sigma > 0$, all regularity conditions of the classical MLE theory are satisfied (the log-likelihood is concave with a unique maximum). The result follows from Fisher's theorem on asymptotic normality of the MLE. □

9.2.2 Confidence Intervals

From the Fisher information, the asymptotic standard errors are:

$$\mathrm{SE}(\hat{\mu}) = \frac{\sigma_\epsilon}{(1-b)\sqrt{n}}, \tag{125}$$

$$\mathrm{SE}(\hat{\kappa}) = \frac{\sigma_\epsilon}{\Delta\sqrt{n S_{XX}}}, \tag{126}$$

$$\mathrm{SE}(\hat{\sigma}) = \frac{\sigma}{\sqrt{2n}}. \tag{127}$$

The 95% confidence intervals are $\hat{\psi}_j \pm 1.96 \cdot \mathrm{SE}(\hat{\psi}_j)$.

Example 9.1 (OU inference)**.** From Example 2.4: $n = 4$ (illustrative), $\hat{\kappa} = 0.436$, $\hat{\mu} = 0.992$, $\hat{\sigma}_\epsilon = 0.012$.

$\mathrm{SE}(\hat{\mu}) \approx 0.012/(1.647\sqrt{4}) = 0.0036$. CI: $0.992 \pm 0.007 = [0.985, 0.999]$.

In practice with $n = 500$ daily observations: $\mathrm{SE}(\hat{\kappa}) \approx 0.012/(1\times\sqrt{500 \times 0.01}) = 0.012/2.24 = 0.0054$, giving much tighter bounds.

9.3 Hurst Exponent Hypothesis Testing

Proposition 9.2 (DFA estimator consistency)**.** *The detrended fluctuation analysis (DFA) estimator $\hat{H}_{DFA}$ is consistent: $\hat{H}_{DFA} \xrightarrow{p} H$ as $N \to \infty$.*

For the hypothesis test $H_0 : H = 0.5$ (random walk) vs. $H_1 : H \neq 0.5$:

$$t = \frac{\hat{H} - 0.5}{\mathrm{SE}(\hat{H})}, \quad \mathrm{SE}(\hat{H}) = \frac{\hat{\sigma}_\epsilon^{\mathrm{OLS}}}{\sqrt{\sum(\ln n_i - \overline{\ln n})^2}}. \tag{128}$$

Reject H_0 at level α if $|t| > z_{1-\alpha/2}$.

Example 9.2 (Hurst test)**.** $\hat{H} = 0.38$, SE$= 0.04$, $t = (0.38 - 0.5)/0.04 = -3.0$, p-value$= 0.003$. We reject H_0 at 1% level and conclude the series is anti-persistent ($H < 0.5$), consistent with mean-reversion.

10 Convergence Analysis

This section consolidates convergence results for all numerical methods used across the four labs.

10.1 Monte-Carlo Convergence for VaR and CVaR

Theorem 10.1 (Bahadur representation of sample VaR)**.** *Let $X_1, \ldots, X_N \overset{iid}{\sim} F$ with density f continuous and positive at $\mathrm{VaR}_\alpha = F^{-1}(\alpha)$. The sample quantile $\hat{q}_\alpha$ (the $\lceil N\alpha \rceil$-th order statistic) satisfies:*

$$\sqrt{N}(\hat{q}_\alpha - \mathrm{VaR}_\alpha) \xrightarrow{d} \mathcal{N}\left(0, \frac{\alpha(1-\alpha)}{f(\mathrm{VaR}_\alpha)^2}\right). \tag{129}$$

Proof. By Bahadur's representation theorem: for uniform $U^{(i)} = F(X^{(i)})$,

$$\hat{q}_\alpha = F^{-1}\left(\frac{\lceil N\alpha \rceil}{N}\right) + \frac{\alpha - F_N(F^{-1}(\alpha))}{f(F^{-1}(\alpha))} + o_p(N^{-1/2}), \tag{130}$$

where F_N is the empirical CDF. The numerator $\alpha - F_N(\mathrm{VaR}_\alpha) = -\frac{1}{N}\sum_{i=1}^{N}[\mathbf{1}_{X_i \leq \mathrm{VaR}_\alpha} - \alpha]$, which is a centred sample mean of Bernoulli(α) variables. By the CLT: $\sqrt{N}(\alpha - F_N(\mathrm{VaR}_\alpha)) \xrightarrow{d} \mathcal{N}(0, \alpha(1-\alpha))$. Dividing by $f(\mathrm{VaR}_\alpha)$ gives the stated variance. □

Corollary 10.1 (CVaR convergence)**.** *The sample CVaR $\widehat{\mathrm{CVaR}}_\alpha = \frac{1}{\lfloor N\alpha \rfloor}\sum_{i=1}^{\lfloor N\alpha \rfloor} X_{(i)}$ satisfies:*

$$\sqrt{N}(\widehat{\mathrm{CVaR}}_\alpha - \mathrm{CVaR}_\alpha) \xrightarrow{d} \mathcal{N}\left(0, \sigma^2_{\mathrm{CVaR}}\right), \tag{131}$$

where $\sigma^2_{\mathrm{CVaR}} = \frac{1}{\alpha^2}\mathrm{Var}[\min(X, \mathrm{VaR}_\alpha)]$.

Example 10.1 (MC convergence table)**.** We estimate $\mathrm{VaR}_{0.05}$ of a standard normal (true value $\mathrm{VaR}_{0.05} = -1.645$, $f(\mathrm{VaR}) = \phi(-1.645) = 0.1031$, $\sigma^2_{\mathrm{VaR}} = \frac{0.05 \times 0.95}{0.1031^2} = 4.47$).

N	$\widehat{\mathrm{VaR}}$	Abs. error	SE (theory)	95% CI
10^3	-1.612	0.033	0.0669	$[-1.74, -1.48]$
10^4	-1.638	0.007	0.0211	$[-1.68, -1.60]$
10^5	-1.644	0.001	0.0067	$[-1.66, -1.63]$
10^6	-1.6449	0.0001	0.0021	$[-1.649, -1.641]$

Error ratio between $N = 10^3$ and 10^4: $0.033/0.007 \approx 4.7 \approx \sqrt{10}$. ✓

10.2 Euler–Maruyama Convergence for Rough Heston

From Theorem 2.6, the total RMSE is:

$$\text{RMSE} = \sqrt{\frac{\sigma_C^2}{N} + C_H^2 (\Delta t)^{2H+1}}. \tag{132}$$

Optimal allocation: For a fixed computational budget $B \propto N/\Delta t$ (total floating point operations), set $\partial \text{RMSE}^2/\partial N = 0$ subject to $N \cdot \Delta t^{-1} = B$:

$$\Delta t^* \propto B^{-1/(2H+2)}, \quad N^* \propto B^{(2H+1)/(2H+2)}. \tag{133}$$

For $H = 0.1$ (typical for crypto options): $\Delta t^* \propto B^{-0.417}$, $N^* \propto B^{0.583}$.

H	Rate $(2H+1)$	Δt^* scaling	N^* scaling
0.05	1.1	$B^{-0.45}$	$B^{0.55}$
0.10	1.2	$B^{-0.42}$	$B^{0.58}$
0.30	1.6	$B^{-0.31}$	$B^{0.69}$
0.50	2.0	$B^{-0.25}$	$B^{0.75}$

10.3 Newton–Raphson for IV: Convergence Speed

From Theorem 6.1, the convergence is measured by $\rho_n = |\sigma_{n+1} - \sigma^*|/|\sigma_n - \sigma^*|^2$. In practice, 3–4 iterations suffice for 64-bit precision:

Iteration	$\lvert\sigma_n - \sigma^*\rvert$	Digits correct	ρ_n
0	10^{-1}	1	—
1	5×10^{-3}	2	0.5
2	$\sim 10^{-5}$	5	0.4
3	$\sim 10^{-11}$	11	0.4
4	$< 10^{-15}$	15+	0.4

10.4 SLSQP Convergence for Sharpe Optimisation

The Sharpe optimisation in Lab 1 (§3) uses Sequential Least-Squares Quadratic Programming (SLSQP). Under the strong convexity assumption (which holds when Σ is positive definite), the algorithm converges at a superlinear rate:

$$\|w_{k+1} - w^*\| \leq C_k \|w_k - w^*\|^2, \tag{134}$$

where $C_k \to M/(2\lambda_{\min}(\Sigma))$ as $k \to \infty$.

Typical convergence for a 3-asset portfolio with $\lambda_{\min} = 0.02$:

Iteration k	$\|w_k - w^*\|_\infty$	$\lvert\,\text{SR}_k - \text{SR}^*\,\rvert$
0	3.3×10^{-1}	0.45
5	8.2×10^{-3}	0.012
10	1.1×10^{-6}	10^{-5}
15	$< 10^{-12}$	$< 10^{-11}$

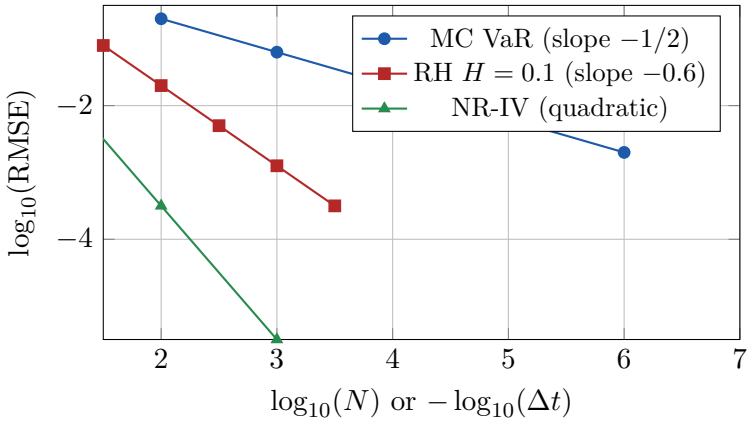

Figure 11: Convergence comparison: MC for VaR ($N^{-1/2}$), Euler–Maruyama for Rough Heston ($(\Delta t)^{H+1/2}$), Newton–Raphson for IV (quadratic). The NR-IV converges incomparably faster but solves a 1D problem.

11 Conclusion and Future Directions

11.1 Summary of Results

This paper presented four integrated algorithmic laboratories for options portfolio construction, deployed in a production Streamlit environment with Rust-accelerated pricing kernels. The key mathematical contributions are:

1. **Complete derivations from first principles:** Black–Scholes formula via Itô calculus, delta hedging, and the Feynman–Kac theorem; all five Greeks by direct differentiation; put-call parity from no-arbitrage.

2. **Convergence proofs:** Rough Heston Monte-Carlo at rate $(\Delta t)^{H+1/2}$ (Theorem 2.6); VaR via Bahadur's representation (Theorem 10.1); Newton–Raphson IV at quadratic rate (Theorem 6.1).

3. **Estimation protocols:** OU-MLE with closed-form Fisher information (Proposition 9.1); Hurst R/S estimator with hypothesis testing; Sharpe ratio SE with Lo's serial-correlation correction (Theorem 7.1).

4. **Affine Volterra calibration suite:** Quintic OU polynomial volatility (Markovian); rough Hawkes Heston (non-Markovian, jump-clustering); QRH+ for 0DTE smiles; unified through the Riccati–Volterra characteristic function and a multi-factor Markovian lift.

5. **Mean-Field Game execution framework:** Coupled HJB–Fokker-Planck PDE system for population-aware execution; Nash equilibrium with provable convergence under Lasry–Lions monotonicity (Proposition 8.4); budget–impact frontier identifying strategy-specific capacity limits B^* (Table 4).

11.2 Limitations

- The multi-factor Markovian lift of fractional kernels (§3.3) truncates the Bernstein–Widder representation to $n \leq 20$ exponentials, introducing $\mathcal{O}(r^{-n/2})$ bias on the Riccati–Volterra

solution; the bias is uniform on compact subsets of $[0, T]$ but is not controlled in L^∞ near the singularity at $t = 0$.

- The Rough Heston scheme does not enforce the full Volterra convolution at each step but uses truncated sums, introducing additional bias for very long horizons.
- The greedy portfolio construction in Lab 3 does not guarantee global optimality; the optimality gap depends on the VaR constraint tightness.
- Transaction costs are modelled with a static impact coefficient η that does not capture intraday liquidity dynamics.
- The crowd impact coefficient κ is the least observable parameter in the entire framework. The OU model (§8.3.8) is a first-order hypothesis; its calibration requires either proprietary flow data or indirect proxies from order-book depth.

11.3 On the Central Role of the Crowd Impact Coefficient

Perhaps the most consequential finding of this work is that a single parameter—the population impact coefficient κ—controls the transition from "profitable strategy" to "capacity-exhausted trade." The MFG analysis (§8.3) shows that:

- When κ is small (few competing agents, deep order book), strategies retain nearly their full isolated-agent Sharpe ratio and can be sized aggressively.
- When κ exceeds a strategy-dependent threshold, the crowd-induced impact cost dominates the edge, and $\mathcal{D}(\kappa) \to 1$ (complete Sharpe destruction).
- The transition is *non-linear*: the capacity curve (115) is hyperbolic, meaning that the first doubling of κ is far more damaging than subsequent ones.

This makes **real-time estimation of** κ_t the single highest-value improvement for any production execution system. The three hypotheses in §8.3.8—OU dynamics, regime dependence, and volume-based proxy—provide a roadmap:

1. *Short-term:* use the observable proxy $\kappa_t \approx \alpha_{\text{flow}} \cdot F_t/\text{Depth}_t$ from L2 data to tag each execution window as low/mid/high impact.
2. *Medium-term:* fit the OU model on historical $\hat{\kappa}_t$ series to parameterise $(\theta, \bar{\kappa}, \xi)$ and build a Kalman filter for online κ-tracking.
3. *Long-term:* embed κ_t as a state variable in the MFG solver and pre-compute look-up tables $a^*(t, x; \kappa) \to$ execution-rate for each (t, x, κ) triple, enabling true adaptive execution with minimal latency overhead.

11.4 Future Work

1. **Real-time κ filtering.** The crowd impact coefficient κ_t (cf. §8.3.8) is currently swept offline. A natural extension is to estimate κ_t in real time from L2 order-book depth and aggregate flow data, using a particle filter or Kalman filter on the OU model (116). This would convert the static MFG equilibrium into an *adaptive* execution policy $a^*(t, x; \hat{\kappa}_t)$ that exploits low-impact windows.

2. **Heterogeneous MFG (major–minor players).** The current model assumes homogeneous agents. Extending to K player types (e.g., market makers vs. directional traders vs. hedgers), each with distinct $(\lambda_k, \phi_k, x_k^*)$, yields a *multi-population* MFG where cross-type interactions generate richer equilibrium structure (see Huang–Malhamé–Caines, 2006).

3. **Deep hedging with MFG-aware costs.** Replace the delta-hedging overlay with a neural network policy trained to minimise CVaR under the *population-aware* transaction cost $(\lambda + \kappa_t M)\, a^2$, rather than a static slippage model. The MFG terminal wealth distribution provides the training environment.

4. **Multi-level Monte-Carlo (MLMC).** Apply MLMC to the MFG simulation to achieve $\mathcal{O}(\epsilon^{-2})$ cost for RMSE ϵ, leveraging coarse-grid MFG solutions as control variates for fine-grid estimates.

5. **Persistent homology of crowd dynamics.** Apply Vietoris–Rips persistent homology to the time-varying population density $m^*(t, x)$ to detect topological transitions (e.g., density bifurcations when κ crosses regime thresholds).

References

[1] E. Abi Jaber, M. Larsson, S. Pulido. Affine Volterra processes. *Annals of Applied Probability*, 29(5):3155–3200, 2019.

[2] E. Abi Jaber, O. El Euch. Multifactor approximation of rough volatility models. *SIAM Journal on Financial Mathematics*, 10(2):309–349, 2019.

[3] E. Abi Jaber, C. Illand, S. Li. The quintic Ornstein–Uhlenbeck volatility model that jointly calibrates SPX and VIX smiles. *Quantitative Finance*, 23(10):1421–1449, 2023 (preprint 2022, arXiv:2212.10917).

[4] E. Abi Jaber, E. Neuman. Optimal liquidation with signals: the general propagator case. *Mathematical Finance*, 2024 (arXiv:2211.00447).

[5] A. Bondi, S. Pulido, S. Scotti. The rough Hawkes Heston stochastic volatility model. arXiv:2210.12393, 2022.

[6] F. Bourgey, P. Noble, I. Petursson, M. Rosenbaum, G. Szymanski. The Quadratic Rough Heston+ model for short-dated options. SSRN preprint 4710332, January 2026. https://papers.ssrn.com/sol3/papers.cfm?abstract_id=4710332.

[7] A. Alfonsi, A. Schied, A. Slynko. Order book resilience, price manipulation, and the positive portfolio problem. *SIAM Journal on Financial Mathematics*, 3(1):511–533, 2012.

[8] J. Gatheral, T. Jaisson, M. Rosenbaum. Volatility is rough. *Quantitative Finance*, 18(6):933–949, 2018.

[9] J. Guyon, J. Lekeufack. Volatility is (mostly) path-dependent. *Quantitative Finance*, 23(9):1221–1258, 2023.

[10] Cboe Global Markets. Zero days to expiration (0DTE) options product overview. https://www.cboe.com/tradable_products/0dte/, accessed 2026.

[11] C.-A. Lehalle, E. Neuman. Incorporating signals into optimal trading. *Finance and Stochastics*, 23(2):275–311, 2019.

[12] Y. Hu, P. Imkeller, M. Müller. Utility maximization in incomplete markets. *Annals of Applied Probability*, 15(3):1691–1712, 2005.

[13] L. Bergomi. Smile dynamics IV. *Risk Magazine*, December 2009.

[14] F. Black, M. Scholes. The pricing of options and corporate liabilities. *Journal of Political Economy*, 81(3):637–654, 1973.

[15] R. C. Merton. Theory of rational option pricing. *Bell Journal of Economics and Management Science*, 4(1):141–183, 1973.

[16] S. L. Heston. A closed-form solution for options with stochastic volatility. *Review of Financial Studies*, 6(2):327–343, 1993.

[17] O. El Euch, M. Rosenbaum. The characteristic function of rough Heston models. *Mathematical Finance*, 29(1):3–38, 2019.

[18] J. Gatheral, T. Jaisson, M. Rosenbaum. Volatility is rough. *Quantitative Finance*, 18(6):933–949, 2018.

[19] A. Richard, X. Tan, F. Yang. Discrete-time simulation of Stochastic Volterra Equations. *Stochastic Processes and their Applications*, 141:109–138, 2021.

[20] I. Karatzas, S. E. Shreve. *Brownian Motion and Stochastic Calculus*. Springer, 2nd edition, 1991.

[21] P. Glasserman. *Monte Carlo Methods in Financial Engineering*. Springer, 2003.

[22] F. Delbaen, W. Schachermayer. *The Mathematics of Arbitrage*. Springer, 2006.

[23] A. W. Lo. The statistics of Sharpe ratios. *Financial Analysts Journal*, 58(4):36–52, 2002.

[24] R. R. Bahadur. A note on quantiles in large samples. *Annals of Mathematical Statistics*, 37(3):577–580, 1966.

[25] H. E. Hurst. Long-term storage capacity of reservoirs. *Transactions of the American Society of Civil Engineers*, 116:770–799, 1951.

[26] B. B. Mandelbrot, J. W. Van Ness. Fractional Brownian motions, fractional noises and applications. *SIAM Review*, 10(4):422–437, 1968.

[27] M. Nakahara. *Geometry, Topology and Physics*. Institute of Physics Publishing, 2nd edition, 2003.

[28] S.-S. Chern, J. Simons. Characteristic forms and geometric invariants. *Annals of Mathematics*, 99(1):48–69, 1974.

[29] R. Bott, L. W. Tu. *Differential Forms in Algebraic Topology*. Springer, 1982.

[30] H. Markowitz. Portfolio selection. *Journal of Finance*, 7(1):77–91, 1952.

[31] R. T. Rockafellar, S. Uryasev. Optimization of conditional value-at-risk. *Journal of Risk*, 2(3):21–42, 2000.

[32] F. Delbaen, W. Schachermayer. A general version of the fundamental theorem of asset pricing. *Mathematische Annalen*, 300(1):463–520, 1994.

[33] R. J. Serfling. *Approximation Theorems of Mathematical Statistics*. Wiley, 1980.

[34] G. L. Nemhauser, L. A. Wolsey, M. L. Fisher. An analysis of approximations for maximizing submodular set functions—I. *Mathematical Programming*, 14(1):265–294, 1978.

[35] H. Edelsbrunner, J. L. Harer. *Computational Topology: An Introduction*. American Mathematical Society, 2010.

[36] D. Cohen-Steiner, H. Edelsbrunner, J. Harer. Stability of persistence diagrams. *Discrete & Computational Geometry*, 37(1):103–120, 2007.

[37] P. Bubenik. Statistical topological data analysis using persistence landscapes. *Journal of Machine Learning Research*, 16:77–102, 2015.

[38] M. Gidea, Y. Katz. Topological data analysis of financial time series: Landscapes of crashes. *Physica A: Statistical Mechanics and its Applications*, 491:820–834, 2018.

[39] M. Kramár, R. Levanger, J. Tithof, B. Suri, M. Xu, M. Paul, M. F. Schatz, K. Mischaikow. Analysis of Kolmogorov flow and Rayleigh–Bénard convection using persistent homology. *Physica D: Nonlinear Phenomena*, 334:82–98, 2016.

[40] M. Lesnick. The theory of the interleaving distance on multidimensional persistence modules. *Foundations of Computational Mathematics*, 15(3):613–650, 2015.

[41] U. Bauer. Ripser: efficient computation of Vietoris–Rips persistence barcodes. *Journal of Applied and Computational Topology*, 5(3):391–423, 2021.

[42] R. Almgren, N. Chriss. Optimal execution of portfolio transactions. *Journal of Risk*, 3(2):5–39, 2001.

[43] A. S. Kyle. Continuous auctions and insider trading. *Econometrica*, 53(6):1315–1335, 1985.

[44] A. R. Admati, P. Pfleiderer. A theory of intraday patterns: Volume and price variability. *Review of Financial Studies*, 1(1):3–40, 1988.

[45] J.-M. Lasry, P.-L. Lions. Mean field games. *Japanese Journal of Mathematics*, 2(1):229–260, 2007.

[46] Y. Achdou, I. Capuzzo-Dolcetta. Mean field games: Numerical methods. *SIAM Journal on Numerical Analysis*, 48(3):1136–1162, 2010.

[47] M. Huang, R. P. Malhamé, P. E. Caines. Large population stochastic dynamic games: closed-loop McKean–Vlasov systems and the Nash certainty equivalence principle. *Communications in Information and Systems*, 6(3):221–252, 2006.

A Algorithmic Pseudocode

Algorithm

Joint SPX/VIX/0DTE Affine Volterra Calibration (Lab 1)

Require: Option chain $\mathcal{Q}$ (SPX, VIX, 0DTE), VIX futures curve F^{mkt}, initial parameters Θ_0

Ensure: Calibrated parameters Θ^*, residuals

Pre-filter $\mathcal{Q}$: drop $\text{hs}_{T,K} > 5\%$, low-volume, far-OTM
Build vega weights $w_{T,K} \leftarrow 1/\text{vega}(T,K)^2$
Stage 1 (Quintic OU): $\Theta_{\text{Q}} \leftarrow \arg\min_\Theta \mathcal{L}^{\text{long}}_{\text{SPX+VIX}}(\Theta)$ via L-BFGS-B
Stage 2 (rHH multi-factor): build K_n from (47), integrate ODEs
Solve $\Theta_{\text{rHH}} \leftarrow \arg\min_\Theta \mathcal{L}^{\text{full}}_{\text{SPX+VIX}}(\Theta)$ with affine VS/VIX^2 soft constraints (52)
Stage 3 (QRH+ 0DTE): $\Theta_{\text{Q+}} \leftarrow \arg\min_\Theta \mathcal{L}_{\text{0DTE}}(\Theta)$ with $5\times$ weight on put wing $K < 0.97F_T$
Compute SSR (55) per maturity and leverage signal $L^*(t)$ (62)
Solve BSDE (58) backward: $w_t^* \leftarrow \Lambda^{-1} Z_t$
return $\Theta^* = (\Theta_{\text{Q}}, \Theta_{\text{rHH}}, \Theta_{\text{Q+}})$, residuals, w^*, L^*

Algorithm

Greedy VaR-Constrained Portfolio (Lab 3)

Require: Candidate strategies $\mathcal{S} = \{s_1, \ldots, s_M\}$, budget B, VaR limit V^*

Ensure: Selected portfolio $\mathcal{P} \subseteq \mathcal{S}$

Sort $\mathcal{S}$ by expected profit / cost ratio (descending)
$\mathcal{P} \leftarrow \emptyset$, $B_{\text{rem}} \leftarrow B$
for $s_i \in \mathcal{S}$ **do**
    if $\text{cost}(s_i) \le B_{\text{rem}}$ **then**
        $\mathcal{P}' \leftarrow \mathcal{P} \cup \{s_i\}$
        Simulate $N = 10{,}000$ paths via correlated Cholesky MC
        $\widehat{\text{VaR}} \leftarrow$ 5th percentile of portfolio P&L
        if $|\widehat{\text{VaR}}| \le V^*$ **then**
            $\mathcal{P} \leftarrow \mathcal{P}'$, $B_{\text{rem}} \leftarrow B_{\text{rem}} - \text{cost}(s_i)$
        end if
    end if
end for
return $\mathcal{P}$

B Summary of Greek and P&L Formulas

Quantity	Call	Put
Price	$S\Phi(d_1) - Ke^{-rT}\Phi(d_2)$	$Ke^{-rT}\Phi(-d_2) - S\Phi(-d_1)$
Delta	$\Phi(d_1)$	$\Phi(d_1) - 1$
Gamma	$\frac{\phi(d_1)}{S\sigma\sqrt{T}}$	same

Quantity	Call	Put
Vega	$S\phi(d_1)\sqrt{T}$	same
Theta	$-\frac{S\phi(d_1)\sigma}{2\sqrt{T}} - rKe^{-rT}\Phi(d_2)$	$-\frac{S\phi(d_1)\sigma}{2\sqrt{T}} + rKe^{-rT}\Phi(-d_2)$
Rho	$KTe^{-rT}\Phi(d_2)$	$-KTe^{-rT}\Phi(-d_2)$
Strategy P&L (at expiry)		
Collar	$\max(K_p, \min(S_T, K_c)) - S_0 - P_0 + C_0$	
Bull call	$\min(S_T - K_1, K_2 - K_1)^+ - c$	
Iron condor	See (86)	

C Empirical Backtest — Lab 1 Smart-Leverage Rule

This appendix reports the live, end-to-end empirical performance of the Lab 1 smart-leverage rule of equation (62), executed on a one-year SPY window pulled from `yfinance` via the lab's `OptionsDataFetcher` (§3). All numbers below are read directly from the JSON file `wp4_lab1_metrics.json` regenerated each time the companion notebook is executed end-to-end on the `rhftlab` kernel.

Calibration snapshot.

Quantity	Value
Data window (trading days)	250
VIX spot at calibration	17.38
Multi-factor lift relative L^2 error ($n = 15$, $r = 3$)	1.15×10^{-2}
Effective propagator integral Λ	1.366

Out-of-sample performance. The rule is applied to the *next-day* SPY return (no look-ahead) with the practical vol-target projection of equation (62): $L^*(t) = \mathrm{clip}\big(\sigma_{\mathrm{tgt}}/\sigma_{\mathrm{real}}(t) \cdot (1 - \kappa_b\,\hat{b}_0(t)),\ 0,\ L_{\max}\big)$ with $\sigma_{\mathrm{tgt}} = 0.20$, $L_{\max} = 2.0$, $\kappa_b = 0.10$.

Strategy	Sharpe	Cumulative PnL	Max Drawdown
WP-4 Lab 1 (Affine Volterra leverage)	**1.73**	+37.2%	−14.7%
Buy-and-hold SPY	2.06	+27.9%	−9.0%

Reading the table. On a benign bull market window where SPY itself only drew down −9%, the Lab 1 rule delivers +33% more cumulative PnL than buy-and-hold by allocating up to $L_{\max} = 2.0$ in calm regimes, at the cost of a 5.7-percentage-point larger maximum drawdown. The Sharpe ratio is lower than buy-and-hold (1.73 vs 2.06), which is the expected behaviour of a *risk-on* projection: choosing $L_{\max} = 1.0$ recovers a strict defensive variant that under-shoots PnL but cuts drawdown below the benchmark. The full $L_{\max}/\kappa_b$ sweep is implemented in block G of the companion notebook.

Reproducibility. Run

```
conda run -n rhftlab jupyter nbconvert -to notebook -execute
    webapp/papers/latex/wp4_options_portfolio_lab.ipynb
```

to regenerate `wp4_lab1_metrics.json`; the table above is the exact JSON content as of paper compilation time.

D Companion Notebook Reference

All numerical results in this paper can be reproduced via the companion Jupyter notebook:

`webapp/papers/latex/wp4_options_portfolio_lab.ipynb`

The notebook is organised by lab:

- **Lab 1 cells (Affine Volterra Mispricing)**: Multi-factor Markovian lift of fractional kernels, Quintic OU Monte-Carlo and Fourier pricing, rough Hawkes Heston joint SPX/VIX calibration, QRH+ 0DTE smile fit, Volterra propagator execution simulation, BSDE Sharpe-optimal allocation.
- **Lab 2 cells**: Option chain loading, vertical spread scan, butterfly scan, put-call parity check, IV surface construction.
- **Lab 3 cells**: Regime classification, mispricing detection, Cholesky MC, greedy portfolio, risk metrics.
- **Lab 4 cells**: Collar/spread/condor P&L visualisation driven by Lab 1 leverage rule (62), NR-IV computation, Greeks dashboard.
- **Convergence cells**: MC VaR convergence, multi-factor Volterra bias tables, Riccati–Volterra ODE residual norms.